

Ion-Neutralization Spectroscopy of Solids and Solid Surfaces

HOMER D. HAGSTRUM

Bell Telephone Laboratories, Murray Hill, New Jersey

(Received 12 May 1966)

A new method of spectroscopy of solids is presented. By means of it, information concerning the state densities in solids is extracted from measured kinetic-energy distributions of electrons ejected from the solid by slow noble-gas ions. The basic electronic process involved is the radiationless, two-electron, Auger-type transition which neutralizes the ion to its ground state at the atomically clean solid surface and simultaneously excites another electron in the solid. The method starts with measured energy distributions and, making a minimum of assumptions, works its way back to what may be called the transition density function. This function, which specifies the relative probability that an electron at a given band energy will be involved in the neutralization process, depends on state densities in initial and final states of the process, transition probability, final-state interaction, and other factors. The information obtained is of the same general kind as that obtained by soft-x-ray spectroscopy and photoelectron spectroscopy. When the surface is atomically clean the transition density involves bulk-state densities and transition probabilities which depend on the surface. For surfaces with monolayers involving foreign atoms, the transition density is modified by the state-density and wave-function changes resulting from the presence of the two-dimensional surface crystal. The method, feasibility, and characteristics of the ion-neutralization spectroscopy are discussed using experimental data for copper and nickel as illustrative examples. Experimental apparatus and operating conditions are discussed only briefly.

I. INTRODUCTION

A NEW method of electronic spectroscopy of solids and solid surfaces is presented in this paper. Like any spectroscopy of an atomic system it is based on an electronic transition process and its results involve not only the distribution in energy of allowed quantum states of the system but factors which depend on the characteristics of the basic transition process. For a condensed system such as the crystalline solid of interest here we expect an electronic spectroscopy to involve the densities of filled and unfilled valence states, the transition probability of the electronic process, as well as final-state interactions including possible many-body effects.

The experimental results of any spectroscopy of solids are expressible in terms of a function of band energy which we shall call the transition density. This is a function which gives the relative probability that an electron at the specified band energy will be involved in the transition process and it includes all the possible factors listed above. Having the transition density we are faced with the problem of trying to evaluate its components in order to draw conclusions concerning the density of electronic states in the solid. Thus it is evident that the development of several electronic spectroscopies of solids is important. Each will have its peculiar transition probability and final-state-interaction factors, so that intercomparison of results should prove fruitful.

The ion-neutralization spectroscopy (INS) discussed in this paper is based on the two-electron, Auger-type process which occurs when a slow ion of large neutralization energy (ionization energy of the parent atom) is neutralized at the solid surface. The method has developed out of an extended series of experimental and interpretive studies of the neutralization of slow ions at

solid surfaces.¹⁻³ The "spectroscopic information" is extracted from measured kinetic-energy distributions of electrons ejected from the solid in the ion-neutralization process. That there is information about the solid in such distributions may be seen in Figs. 1 and 2. In

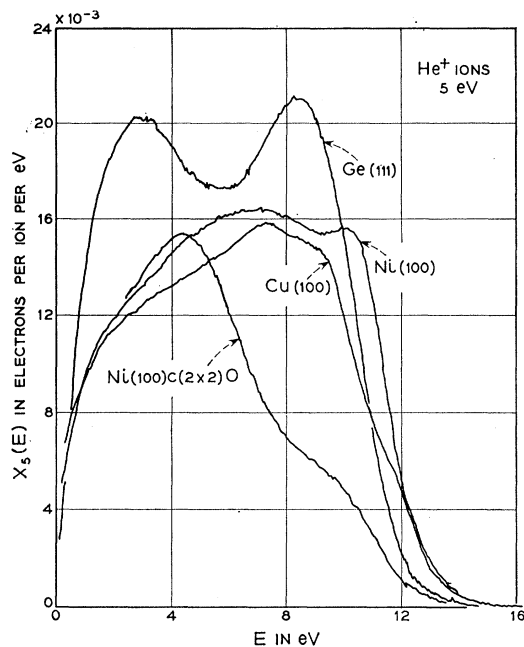


Fig. 1. Kinetic-energy distributions of electrons ejected by 5-eV He^+ ions from the atomically clean faces of Ge(111), Ni(100), Cu(100), and a Ni(100) face having the $c(2 \times 2)$ structure of Ni and O on its surface. These are tracings of X - Y recorder plots of analog derivatives of electron retarding potential characteristics.

¹ H. D. Hagstrum, *Phys. Rev.* **96**, 336 (1954).

² H. D. Hagstrum, *Phys. Rev.* **122**, 83 (1961).

³ H. D. Hagstrum, Y. Takeishi, and D. D. Pretzer, *Phys. Rev.* **139**, A526 (1965).

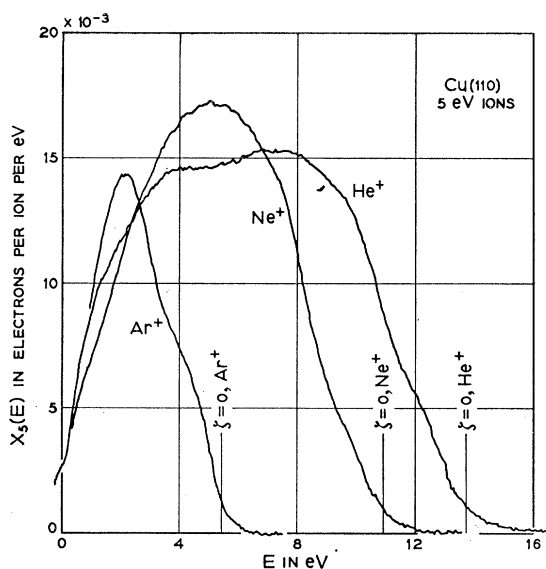


FIG. 2. Electron kinetic-energy distributions for three ions of different neutralization energy (ionization energy of parent atom) incident on the same crystal face. Note how structure features shift on the E scale with effective neutralization energy but remain fixed relative to the maximum energy of the curve, the zero of the scale of band energy, ζ . The $\zeta=0$ point is determined, as indicated in the text of Secs. III and VI, as the point where the extrapolated $X_0(E)$ distribution starts from zero.

Fig. 1 several distributions are shown for the same ion incident on several solids. Quite different distributions are obtained. Clearly the ion-neutralization process differs from secondary electron emission by primary electrons for which the kinetic-energy distribution has a form which is essentially independent of the solid. In Fig. 2 are shown distributions for the (110) face of copper obtained for the three noble-gas ions, He^+ , Ne^+ , and Ar^+ . Note how the same structure features appear at comparable points in the curves relative to the maximum energy of each curve. As we shall see, this is direct evidence that these features arise from structure in the initial state of the process, namely, the filled valence band of the solid.

Experimental data of the type shown in Figs. 1 and 2 have been obtained in collaboration with G. E. Becker, D. D. Pretzer, and Y. Takeishi. Papers have been published presenting experimental studies of the ion-neutralization process for nickel,⁴ germanium,⁵ and gallium arsenide.⁶ Although digital data of the required quality were available, reduction of them by the methods of INS was not attempted in these papers. This will be done in subsequent publications. A preliminary report of the application of INS to data for copper and nickel has been published.⁷

⁴ Y. Takeishi and H. D. Hagstrum, *Phys. Rev.* **137**, A641 (1965).

⁵ Y. Takeishi and H. D. Hagstrum, *Surface Sci.* **3**, 175 (1965).

⁶ D. D. Pretzer and H. D. Hagstrum, *Surface Sci.* **4**, 265 (1966).

⁷ H. D. Hagstrum and G. E. Becker, *Phys. Rev. Letters* **16**, 230 (1966).

Since the basic process of INS occurs at the surface of the solid it will be necessary in this paper to discuss in some detail the role of the surface. We will be interested in two types of surface: a , one that is atomically clean annealed and well ordered, and b , one that includes foreign atoms as well as substrate atoms in a crystallographically ordered phase, one monolayer thick, attached to an otherwise clean substrate. In discussing INS for these cases it is essential that the meaning of the terms "density of states" and "transition probability factors" be kept clearly in mind. For a crystal having no specifically surface states and no band bending, an electron in a given electronic state has access to the entire crystal, including the surface layers and a limited region extending into the vacuum outside. This is true whether the surface is type a or b listed above. The wave function extends throughout the crystal, having an exponentially decreasing tail outside the surface. Thus the density of states is the same throughout the bulk and surface regions and, for the same solid, can depend only very slightly (ca. one part in 10^7) on whether the surface is type a or b . Wave-function magnitudes in the surface region, however, will differ markedly from those in the bulk and will also depend strongly on whether the surface is of type a or b . This will affect the magnitude of the matrix element of the process and hence the transition probability. Provided final-state interactions and many-body effects are not strong, evaluation of the principal wave-function modifications for the clean surface leads to conclusions concerning the bulk density of states for the clean crystal (Sec. VIII). Results for the crystal with surface b , used in conjunction with the results for surface a , give information about the electronic states introduced by the ordered surface monolayer (Sec. X). Furthermore, *bona fide* surface states on semiconductor surfaces should be observable if they are filled. Band bending at the surface will usually be so gradual relative to the region in which the Auger electron is excited as to have negligible effect.

INS produces data of the same general type as soft-x-ray spectroscopy (SXS)⁸⁻¹¹ and photoelectron spectroscopy (PES) based on photoelectric-emission processes for which k conservation is not important.^{12,13} Band-structure information is also obtainable from photoelectric-emission studies for which k conservation is important¹⁴⁻¹⁶ and from optical-constant data,¹⁷ although in these cases one does not derive a transition-

⁸ D. H. Tomboulion, in *Handbuch der Physik*, edited by S. Flügge (Springer-Verlag, Berlin, 1959), Vol. 30, pp. 246-304.

⁹ L. G. Parratt, *Rev. Mod. Phys.* **31**, 616 (1959).

¹⁰ H. Niehrs, *Ergeb. Exakt. Naturw.* **23**, 359 (1950).

¹¹ H. W. B. Skinner, *Rept. Progr. Phys.* **5**, 257 (1939).

¹² C. N. Berglund and W. E. Spicer, *Phys. Rev.* **136**, A1044 (1964).

¹³ A. J. Blodgett, Jr., and W. E. Spicer, *Phys. Rev.* **146**, 390 (1966).

¹⁴ G. W. Gobeli and F. G. Allen, *Phys. Rev.* **137**, A245 (1965).

¹⁵ F. G. Allen and G. W. Gobeli, *Phys. Rev.* **144**, 558 (1966).

¹⁶ W. E. Spicer, *Phys. Rev. Letters* **11**, 243 (1963).

¹⁷ H. Ehrenreich, H. R. Philipp, and D. J. Olechna, *Phys. Rev.* **131**, 2469 (1963).

density function for the filled band in the sense used here.

The plan of this paper is as follows: In Sec. II we discuss the ion-neutralization process on which INS is based. The basic plan of INS is presented in Sec. III, followed by a discussion of its experimental feasibility in Sec. IV. The discussion of the theoretical feasibility of the method is introduced in Sec. V and carried out in Secs. VI-IX. The effect on INS of foreign atoms in an ordered surface monolayer is discussed in Sec. X and the over-all characteristics of the INS method are summarized in Sec. XI in which comparisons with other solid-state spectroscopies are also made.

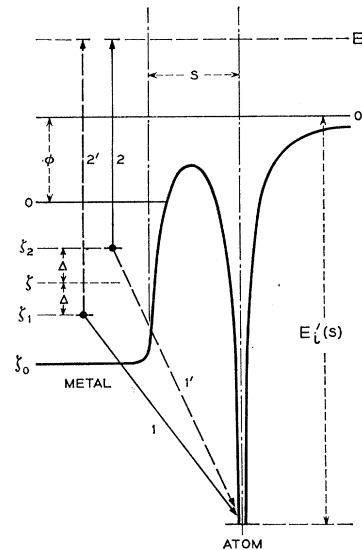
II. THE ION-NEUTRALIZATION PROCESS

The electronic transition process basic to INS is illustrated in the energy-level diagram of Fig. 3. In the presence of the incoming ion outside the surface two electrons in the filled valence band of the solid interact, exchanging energy and momentum. One electron, which we shall call the neutralizing or "down" electron, tunnels through the barrier and drops into the vacant atomic level. The energy released in this transition (1 or 1' in Fig. 3) is taken up by the second electron, termed the excited or "up" electron, which then rises on the energy diagram. This exciting transition (2 or 2' in Fig. 3) carries the second electron to the energy E above the vacuum level. The atomic ground state lies at an energy $E_i'(s)$ below the vacuum level. $E_i'(s)$ is the energy required to ionize the parent atom at the distance s from the solid surface and is less than the free-space ionization energy by virtue of interaction of the neutral and ionized states with the solid. Two pairs of transitions, (1,2) and (1',2'), which bear an exchange relation to each other, can be distinguished. We shall discuss these exchange transitions and their matrix elements later (Sec. VIII). At the moment we focus attention on the (1,2) transitions only. For these the down electron gives up an amount of energy $E_i'(s_i) - \varphi - \zeta_1$, where $E_i'(s)$ is evaluated for the ion-solid separation s_i at which the electronic transitions occur. The up electron acquires this amount of energy in the radiationless process. The energy by which the up electron is excited may also be written as $E + \varphi + \zeta_2$. Equating these energy expressions we obtain

$$E = E_i'(s_i) - (\zeta_1 + \varphi) - (\zeta_2 + \varphi). \quad (1)$$

Since ζ_1 and ζ_2 may lie anywhere in the filled band we expect a band of excited electrons. Some of these may, if properly directed, surmount the surface barrier and leave the solid. Outside, their kinetic-energy distribution may be measured. Our task in this section is to understand the factors which determine the form of this distribution. We note that the ion-neutralization process is a radiationless process of an Auger type. It has been discussed in some detail in earlier publications.^{1,2} Resonance tunneling into excited states discussed in

FIG. 3. Energy-level diagram of a metal with an ion just outside its surface. The electron transition pairs (1,2) and (1',2') illustrate the Auger-type transitions of the ion-neutralization process. Final electron energy E is measured from zero at the vacuum level. The energies of initial states in the filled band, ζ , are measured positively down into the band from the top of the band (Fermi level for a metal, φ eV below the vacuum level).



these earlier papers does not play a fundamental role in this work.

We now proceed to introduce the functions needed to discuss the Auger neutralization process and the method of INS based upon it. These functions are shown in Fig. 4 using a somewhat different notation from previous publications but one more suited to the present work. Curves for He^+ , Ne^+ , and Ar^+ are shown. We consider first the curves for He^+ and simplify the discussion at this point by assuming that all transition-probability or matrix-element factors are constant, independent of band energy ζ and of symmetry character of the band electrons. We also neglect, for the moment, the effects of exchange-matrix-element cancellation and final-state interactions, and assume equal transition probability factors for the up and down electrons. As we shall see, these assumptions require that (1) there be a very thin barrier between ion and solid, (2) all band electrons have the same symmetry, and (3) the matrix element require both up and down electrons to originate in identical regions at the solid surface. At this point we will also assume a constant density of final states and neglect energy broadening inherent in the transition process. Under these rather drastic assumptions the probability of involvement of a band electron of energy in the range ζ to $\zeta + d\zeta$ depends solely on density of initial states in the valence band, $N_v(\zeta)$, which is then equal to the function $U(\zeta)$ shown in Fig. 4.

From $U(\zeta)$ in Fig. 4 we wish first to find the internal distribution in energy $F(E)$ of electrons excited in the ion-neutralization process. This is readily derived from the following observation. Excited electrons lying in a range dE at energy E (end of arrow 2 in Fig. 3) may be obtained from any neutralization process for which the initial states of the two participating electrons are symmetrically disposed on either side of the energy ζ lying half-way between E and the ground state of the atom at $-E_i(s_i)$. Values of E and ζ meeting this con-

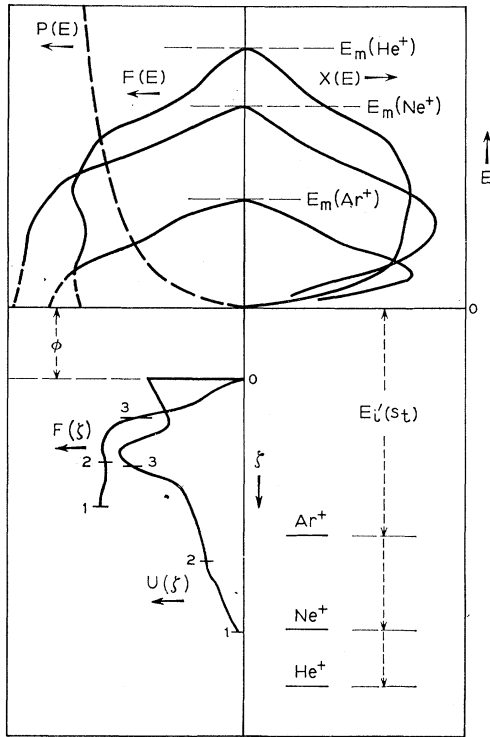


FIG. 4. Energy-level diagram on which are drawn the functions important to an understanding of the ion-neutralization process. Functions are shown which illustrate the division of $X(E)$ by $P(E)$ to get $F(E)$ and $F(\xi)$ for the three ions He^+ , Ne^+ , Ar^+ incident on $\text{Cu}(100)$. Data for He^+ carry $F(\xi)$ to point 1, Ne^+ to point 2, and Ar^+ to point 3. Corresponding points are indicated on the $U(\xi)$ function.

dition satisfy the relation

$$E = E'_i(s_i) - 2(\xi + \varphi) \quad (2)$$

obtained from Eq. (1) by setting $\xi_1 = \xi_2 = \xi$. In Fig. 3 we depict initial states at $\xi_1 = \xi + \Delta$ and $\xi_2 = \xi - \Delta$ which are symmetrically disposed with respect to ξ . The probability of the specific neutralization process involving these states must be proportional to $N_v(\xi + \Delta) \times N_v(\xi - \Delta)$, the product of state densities at the initial energies. Clearly, the total probability of producing an excited electron in dE at E is the integral of this product over the energy increment Δ . Using our more general band function $U(\xi)$, we may write this probability as

$$F(\xi) = \int_0^\xi U(\xi + \Delta) U(\xi - \Delta) d\Delta. \quad (3)$$

The internal energy distribution $F(E)$ is obtained from $F(\xi)$ merely by changing the energy variable according to Eq. (2) and normalizing above the Fermi level to an area equal to one electron per incident ion.

$F(\xi)$ is the self-convolution, convolution square, or fold of the function $U(\xi)$. $F(\xi)$ may be termed the pair density function for all electron pairs in the initial band which can produce an excited Auger electron at

$E = E'_i - 2(\xi + \varphi)$. If the matrix-element, final-state-density, and final-state-interaction factors are included in $U(\xi)$, then $F(\xi)$ becomes what might be termed the transition density for pairs of electrons appropriate to processes producing excited electrons at $E = E'_i - 2(\xi + \varphi)$. $U(\xi)$ then is the transition density for the individual electrons involved. It is interesting to note that $F(\xi)$ related to $U(\xi)$ by Eq. (3) extends to a maximum ξ value half that of the maximum ξ to which $U(\xi)$ is known. We recognize that in the general case $U(\xi)$ may not be the same function for the up and down electrons. Thus we should distinguish a $U_1(\xi)$ and a $U_2(\xi)$ for down and up electrons, respectively, and write

$$F(\xi) = \int_0^\xi U_1(\xi + \Delta) U_2(\xi - \Delta) d\Delta. \quad (4)$$

We discuss these matters in detail in Sec. VIII.

Having the internal distribution of excited electrons, $F(E)$, we can obtain the distribution of externally observed, Auger electrons, $X(E)$, from the probability of electron escape over the surface barrier, $P(E)$, using the expression

$$X(E) = F(E)P(E). \quad (5)$$

The total yield γ of all ejected electrons is the integral of $X(E)$ over all E . The distribution functions $U(\xi)$, $F(\xi)$, $F(E)$, and $X(E)$, as well as the escape probability $P(E)$ are shown in Fig. 4.

We have indicated above what might be termed the "forward model" of the ion-neutralization process by means of which one derives the externally observed yield and electron-energy distribution from functions which characterize the solid and the nature of the electron transition process including escape from the solid. We have indicated that removal of simplifying assumptions would entail a careful interpretation of $U(\xi)$. Energy broadening may be incorporated in the forward model by convolution of $F(E)$ with an energy-broadening function before it is normalized. The general form of $P(E)$ is known but its specific form would have to be derived from data fitting. E'_i is also a parameter of the problem. The forward model has been applied to the case of diamond-type semiconductors.² Specific matrix element factors were included and the several parameters of the problem were determined by fitting calculated yield and external energy distribution to those determined experimentally.

The forward model may be summarized as follows: (1) Devise a parametric form for the state density $N_v(\xi)$ whose general form is known; (2) introduce matrix-element dependences and combine into $U_1(\xi)$, $U_2(\xi)$, or, if appropriate, a single $U(\xi)$; (3) fold $U_1(\xi)$ with $U_2(\xi)$, or $U(\xi)$ with itself, to obtain $F(\xi)$ [Eq. (3) or (4)]; (4) convolute $F(\xi)$ with a broadening function such as a Lorentzian or Gaussian or both; (5) convert $F(\xi)$ to $F(E)$ by the change of variable of Eq. (2); (6) normalize $F(E)$ to one electron per ion per eV in

the range $-\varphi \leq E < \infty$; (7) multiply $F(E)$ by a parametric $P(E)$ to obtain $X(E)$ [Eq. (5)]; (8) sum the area under $X(E)$ to get the total yield γ ; (9) adjust the parameters of the problem to bring agreement between experimental and theoretical $X(E)$ and γ . As we shall now see, our problem in the present work is to reverse the above procedure and to attempt to obtain $U(\zeta)$ from $X(E)$ with a minimum of *a priori* assumptions.

III. THE PLAN OF ION-NEUTRALIZATION SPECTROSCOPY

The "forward" procedure just outlined can work only if the general form of $N_v(E)$ is known. In this case it can give essentially unique results because the several parameters have orthogonal effects on the fit to the experimental data. For diamond-type semiconductors² it yielded information on band structure (width of degenerate p band), on transition probability factors (decrease in probability of electron involvement with increasing angular momentum), and on specific parameters of the neutralization process (effective ionization energy E_i'). However, development of a spectroscopy which extracts information about $U(\zeta)$ from the measured $X(E)$ requires a feasible reverse procedure. We outline the structure of such a procedure in this section and then examine its experimental, theoretical, and mathematical feasibility in succeeding sections of this paper.

Before going into any details, the skeleton of the INS procedure will be given:

- (1) Obtain experimental $X_K(E)$ distributions for two ion energies K_1 and K_2 .
- (2) Extrapolate from $X_{K_1}(E)$ and $X_{K_2}(E)$ to a "debrodened" distribution $X_0(E)$ having relatively small energy broadening. This extrapolation is to be based on the observation that energy broadening appears to vary linearly with ion velocity.³
- (3) Divide $X_0(E)$ by a parametric $P(E)$ function [Eq. (5)] to obtain the internal distribution $F(E)$, and by changing energy variable to ζ [Eq. (2)] to obtain $F(\zeta)$. The parameters of $P(E)$ are determined by demanding that the $F(\zeta)$ functions obtained for He^+ , Ne^+ , and Ar^+ ions should be essentially coincident in those portions where they overlap.
- (4) Further trim the starting portion of $F(\zeta)$ to correct for inadequacies of the linear $X(E)$ extrapolation in this region and to ensure proper functioning of the unfold procedure.
- (5) Unfold Eq. (3) to obtain $U(\zeta)$ from $F(\zeta)$.

We shall elaborate a little further on this procedure here and then discuss its experimental and theoretical feasibility and justification in subsequent sections.

Earlier studies have shown that the total broadening varies linearly with ion velocity for neutralization processes involving electrons from the solid near the

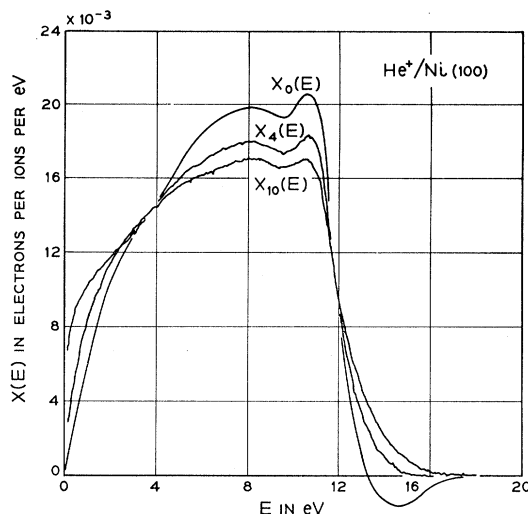


FIG. 5. $X(E)$ distributions for He^+ ions incident on the atomically clean (100) face of nickel. $X_4(E)$ and $X_{10}(E)$ are tracings of X - Y recordings of the distributions for 4 and 10 eV ions, respectively. $X_0(E)$ is a distribution, obtained by linear extrapolation, from which most of the inherent energy broadening has been removed.

top of the valence band.^{3,18} This is made the basis for a linear extrapolation of $X(E)$ from $X_{K_1}(E)$ and $X_{K_2}(E)$ to a function $X_0(E)$ which should be characterized by a considerably reduced amount of energy broadening, at least near the top of the band. The broadening inherent X_{K_1} or X_{K_2} will vary with K_1 and K_2 , of course, but also the specific solid and ion. To minimize the extrapolation we make K_1 as small as experimentally feasible; it is usually 4 or 5 eV. K_2 is usually 10 eV, sufficiently small to keep $X_{K_2}(E)$ in the range of linear broadening but sufficiently different from $X_0(E)$ to avoid introducing large errors in the calculation of the difference distribution $[X_0(E) - X_{K_2}(E)]$.

The linear extrapolation of $X(E)$ may be written thus:

$$X_0(E) = X_{K_1}(E) + R[X_{K_1}(E) - X_{K_2}(E)]. \quad (6)$$

This extrapolation is applied to data for He^+ , Ne^+ , and Ar^+ ions. Adding and subtracting $X_0(E)$ inside the square bracket, we may write for the parameter R

$$R = (X_0 - X_{K_1}) / [(X_0 - X_{K_2}) - (X_0 - X_{K_1})]. \quad (7)$$

In a linear theory for small deviations the differences between a broadened and unbroadened distribution will be proportional to the broadening parameter, that is, the parameter of the broadening function which adds for successive broadenings. This parameter has been shown to be proportional to velocity v or $K^{1/2}$. Then Eq. (7) for the parameter R may be written

$$R_{K_1, K_2} = K_1^{1/2} / (K_2^{1/2} - K_1^{1/2}). \quad (8)$$

¹⁸ H. D. Hagstrum and D. D. Pretzer, in *Proceedings of the Seventh International Conference on Ionization Phenomena in Gases, Belgrade, 1965* (to be published).

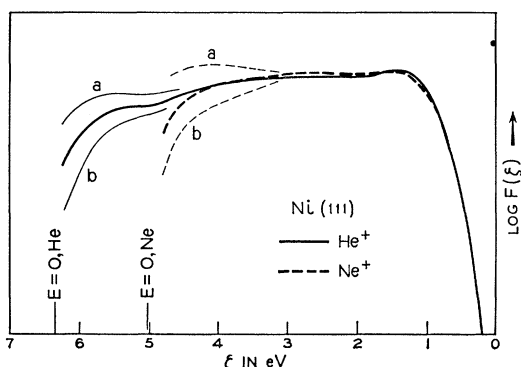


FIG. 6. Figure illustrating how well the parameters of $P(E)$ may be adjusted to give a common $F(\zeta)$. Heavy lines indicate the final result. Curves *a* result if the $P(E)$ function does not rise from zero rapidly enough, curves *b* if it rises too rapidly. The $P(E)$ functions used for He^+ and Ne^+ data rise from zero at the respective $E=0$ points indicated for the two ions.

Specific values calculated from this formula are $R_{4,10}=2.31$ and $R_{5,10}=3.11$. These R values are calculated from incident energies K_1, K_2 which are corrected for ion velocity change near the surface, as is discussed in Sec. VI. The extrapolated distribution $X_0(E)$ and the two experimental distributions from which it is derived are shown for Ni(100) in Fig. 5. We note here that distributions for Ne^+ ions have anomalously large broadening.³ As a consequence smaller R values must be used as is discussed in Sec. VI.

From the "debroadened" external distribution $X_0(E)$ we now determine in step (2) the internal distribution $F(E)$ by dividing by a vacuum level cutoff function $P(E)$ which includes the escape probability and any other dependence on final-state energy E . Thus we are inverting Eq. (5) to obtain

$$F(E) = X_0(E)/P(E). \quad (9)$$

In Fig. 4 X_0, P , and F functions are plotted for the data obtained for He^+, Ne^+ , and Ar^+ ions on Cu(110). Now using Eq. (2) we transform to band energy, obtaining an $F(\zeta)$ function for each ion. That for He^+ extends deepest into the band, that for Ne^+ less, and for Ar^+ least. However, over those ranges of ζ for which data for any two ions overlap we expect $F(\zeta)$ for the two ions to be approximately the same if: (1) $P(E)$ did not change from one ion to the other and we had selected the correct set of parameters, (2) transition probabilities of the Auger processes do not depend on which ion is used, and (3) the density of final states is approximately constant. We have found it possible to find a set of parameters for $P(E)$ which makes $F(\zeta)$ for the three ions have closely the same form to within a multiplicative normalizing constant. How well this is done may be judged from Fig. 6, which shows results for He^+ and Ne^+ ions on Ni(111). Further evidence concerning this is contained in the final unfolding results of Figs. 9 and 10 for different ions. We conclude that $P(E)$ and the transition probabilities do not depend

strongly on the ion used and that the final-state density is a relatively smooth function of E .

In Fig. 4 we have indicated by dashed lines an uncertainty in the $F(E)$ functions near $E=0$. A parametric $P(E)$ function for a limited number of parameters (three have been used here) will be least accurate near $E=0$ where $P(E)$ varies rapidly. Fortunately, the large amount of energy available in the neutralization of He^+ enables us, for metals at least, to obtain the band information we seek using data at E greater than a lower limit of 2 to 4 eV. For E larger than 2 to 4 eV, $P(E)$ varies relatively slowly and three parameters are ample. In fact, considerable deviation from the correct $P(E)$ can be shown to introduce negligible error into the final unfold function $U(\zeta)$. In many cases it would be sufficient to assume $P(E)$ to be constant over the range of data used.

The three-parameter formula we have used for $P(E)$ is

$$P(E) = \frac{1}{2}(1-M)/(1-AM), \quad (10)$$

in which

$$M = \tanh^{-1}BN/\tanh^{-1}B, \\ N = [H/(H+E)]^{1/2}.$$

This formula results if P_Ω ,¹ the angular distribution of excited electrons, is taken to be proportional to the square of the radius of a prolate spheroid which is stepped at the critical angle $\theta_c = \cos^{-1}[H/(H+E)]^{1/2}$, for escape across the surface barrier. The parameters are A , which is related to the magnitude of the step in P_Ω at θ_c and thus to the ratio of matrix elements for escaping and internally reflected electrons; B , which is related to the eccentricity of the ellipsoid and thus the possible matrix element variation within the range $\theta < \theta_c$; and H , the surface-barrier height above the

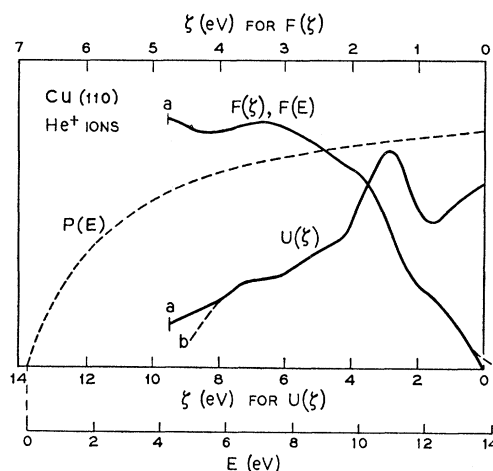


FIG. 7. F, P , and U functions for He^+ ions on Cu(110). Data are cut off at *a* for $E \cong 4$ eV above which point the $P(E)$ function is relatively flat. The difference between the experimental curve and the dashed portion indicated at *b* is probably due to secondary electrons. The $U(\zeta)$ curve shown here and in Figs. 9 and 14 represents the most recent and best data. It differs slightly near $\zeta=6$ eV from that given in Figs. 1 and 3 of Ref. 7.

valence-band bottom. Although there is some rationale behind the derivation of the $P(E)$ of Eq. (10), it should be regarded here purely as a three-parameter formula of the right general shape. Other $P(E)$ functions have been derived and used. They all differ very little from one another for $E > 4$ eV.

The extrapolation procedure of Eq. (6), step (1) above, cannot be expected to give the right answer at or near the high- E end of $X_0(E)$. Because of this and because the subsequent unfolding procedure is very sensitive to the starting form of $F(\zeta)$ near $\zeta=0$ a further extrapolation of the data is required (Sec. IX). This is applied to the $F(\zeta)$ function and consists of a further trimming of the starting portion of the function by at most a few tenths of an eV. Final $F(\zeta)$ functions are shown for copper and nickel in Figs. 7 and 8, respectively.

We now are in possession of an $F(\zeta)$ function which for He^+ ions extends over the longest range of the band energy ζ and agrees quite well over smaller energy ranges with results for Ne^+ and Ar^+ ions. $F(\zeta)$ is to be interpreted either in terms of Eq. (3) or the more general form of Eq. (4). In general we do not have sufficient *a priori* information to solve Eq. (4) for the component functions $U_1(\zeta)$ and $U_2(\zeta)$ of the convolution product. The convolution square of Eq. (3) can be solved for $U(\zeta)$ digitally. We discuss the justification of this procedure in Sec. VIII.

The functions $F(\zeta)$ and $U(\zeta)$ in digital form are

$$F(n\Delta\zeta) = F_n, \quad n=1, 2, 3, \dots, \quad (11)$$

$$U[(2n-1)\Delta\zeta] = U_{2n-1}, \quad n=1, 2, 3, \dots \quad (12)$$

We note that $\Delta\zeta = 0.05$ eV for $\Delta E = 0.1$ eV [Eq. (2)]. A straightforward derivation based on approximating $U(\zeta)$ by a step function with steps centered at the points ζ_{2n-1} leads to what we shall call the step digital

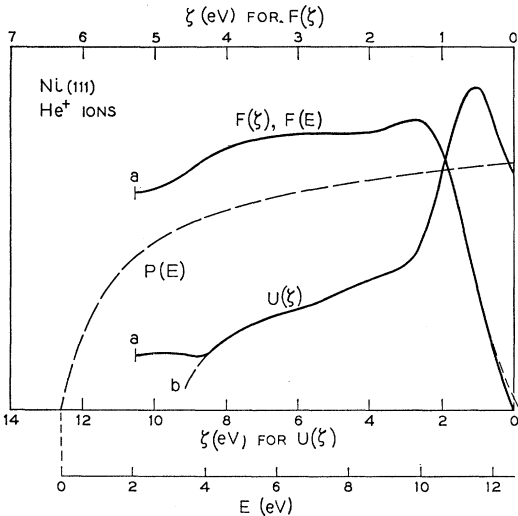


FIG. 8. Curves of F , P , U for He^+ ions on $\text{Ni}(111)$ similar to those of Fig. 7.

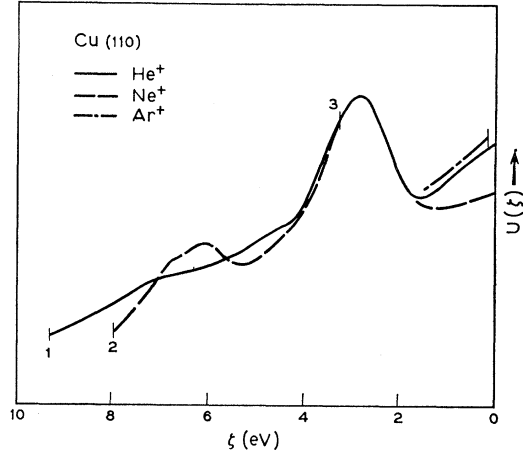


FIG. 9. Comparison of final unfold functions $U(\zeta)$ for He^+ , Ne^+ , and Ar^+ ions on $\text{Cu}(110)$. The R values used in the $X(E)$ extrapolation were $R_{5,10} = 3.11$ for He^+ , $R_{5,10} = 0.2$ for Ne^+ and Ar^+ . Although the He^+ , Ne^+ , and Ar^+ data extend to larger ζ than shown, they are terminated at the points 1, 2, and 3, respectively, as the maximum values to which the data agree and meet one of the basic requirements of the INS data-handling procedure.

fold-unfold relations:

$$F_1 = U_1^2 \Delta\zeta,$$

$$F_2 = 2U_1 U_3 \Delta\zeta,$$

$$F_3 = (U_3^2 + 2U_1 U_5) \Delta\zeta,$$

$$F_4 = (2U_3 U_5 + 2U_1 U_7) \Delta\zeta,$$

$$F_n (n \text{ odd}) = 2\Delta\zeta (U_n^2/2 + U_{n-2} U_{n+2} + U_{n-4} U_{n+4} + \dots + U_1 U_{2n-1}),$$

$$F_n (n \text{ even}) = 2\Delta\zeta (U_{n-1} U_{n+1} + U_{n-3} U_{n+3} + \dots + U_1 U_{2n-1}), \quad (13)$$

and

$$U_1 = (F_1/\Delta\zeta)^{1/2},$$

$$U_3 = (F_2/2\Delta\zeta)/U_1,$$

$$U_5 = (F_3/2\Delta\zeta - U_3^2/2)/U_1,$$

$$U_{2n-1} (n \text{ odd}) = (1/U_1) (F_n/2\Delta\zeta - U_n^2/2 - U_{n-2} U_{n+2} - U_{n-4} U_{n+4} - \dots - U_3 U_{2n-3}),$$

$$U_{2n-1} (n \text{ even}) = (1/U_1) (F_n/2\Delta\zeta - U_{n-1} U_{n+1} - U_{n-3} U_{n+3} - \dots - U_3 U_{2n-3}). \quad (14)$$

The digital unfold [Eqs. (14)] must proceed sequentially since U_n values of lower n appear in expressions for U_n at higher n . We see from Eqs. (11) and (12) that the $U(\zeta)$ function extends over twice the range of ζ of the $F(\zeta)$ function as pointed out earlier. This is a basic characteristic of the fold-unfold relation when written in the form of Eq. (3).

We have thus arrived at a $U(\zeta)$ function derived by the four basic steps of the INS procedure listed above. Examples of data derived from electron distributions for He^+ ions are shown in Figs. 7 and 8. Comparison of final unfold results for different ions on the same target are shown in Figs. 9 and 10. The agreement shown for different ions depends not only on the ability to find

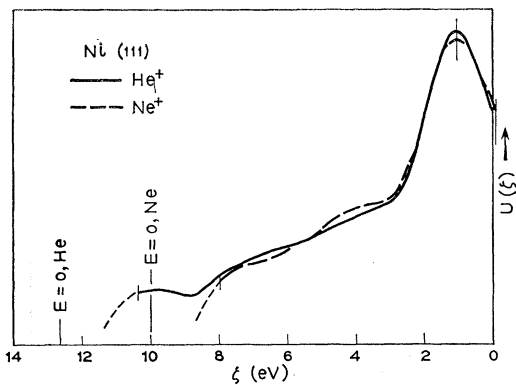


FIG. 10. Comparison of final unfold functions $U(\xi)$ for He^+ and Ne^+ ions on $\text{Ni}(111)$. The R values used in the $X(E)$ extrapolation were $R_{\delta,10}=3.11$ for He^+ and $R_{\delta,10}=1.61$ for Ne^+ .

the parameters for a common $P(E)$ function but also on our use of different R values in Eq. (6) for the different ions. This is discussed further in Sec. VI.

The experimental data are obtained in digital as well as analog form. A first computer program is used to interpolate the data to a convenient even ΔE grid, smooth it, and normalize the area of the $X(E)$ distribution to the measured total electron yield γ . Steps (2), (3), and (5) of the INS procedure are carried out by further computer programs. To date step (4) has been carried out by hand but certainly need not be. In addition to the data smoothing accomplished in the first computer program, further smoothing is done in step (2). The total amount of smoothing can be varied and some study of its effect has been carried out. For the data used in this paper, three 9-point smoothings have been used, one on each of the $X_K(E)$ functions, one on the difference function $X_{K_1}-X_{K_2}$, and one on the final extrapolated function $X_0(E)$. The quality of the digital data for the final unfold $U(\xi)$ may be judged from Fig. 11.

The basic plan of the INS method has now been presented. A more detailed discussion of its experimental feasibility and theoretical justification follows.

IV. EXPERIMENTAL FEASIBILITY OF ION-NEUTRALIZATION SPECTROSCOPY

Experimentally, the feasibility of INS hinges on our ability to obtain $X_K(E)$ energy distributions which are of sufficient accuracy and which have been measured under a demanding set of experimental conditions. The apparatus used in the ion-neutralization measurements is in principle the same as that used in earlier work.¹⁹⁻²¹ However, we are now using a new, mechanically superior, and more versatile apparatus, depicted schematically in Fig. 12. Since no account of this

¹⁹ H. D. Hagstrum, Rev. Sci. Instr. **24**, 1122 (1953).

²⁰ H. D. Hagstrum, Phys. Rev. **119**, 940 (1960).

²¹ H. D. Hagstrum, D. D. Pretzer, and Y. Takeishi, Rev. Sci. Instr. **36**, 1183 (1965).

particular apparatus has been published we shall point out its salient features briefly.

The apparatus depicted in Fig. 12 is enclosed in a metal vacuum envelope in the form of a 3-dimensional right-angle cross of tubing diameter about 16.5 cm. There are four horizontal flanged ports, one port on top, and another on the bottom. The top port carries the target-turning mechanism which (1) can present the target face to any one of the horizontal ports by rotation about axis $A-A$ and (2) can turn the target about the axis $B-B$ through its face. The bottom port connects to the pumps (sputter-ion and mercury diffusion) and a gas-inlet system. The ion-neutralization apparatus bolted to port 1 is like that previously used except for mechanical improvements and a larger sphere S for increased instrumental resolving power. The source end to the left of the septum is independently pumped and has an independent gas-inlet system.

Port 2 carries the target-processing apparatus. The target at the port-2 position may be enclosed in the retractable sphere Sp . Here the target may be sputtered and heated by passing current directly through it. At port 3 the target may be examined by low-energy electron diffraction (LEED). This apparatus is basically the same as the display type in current use²² except that here we look past the target at the pattern on the phosphor-coated glass screen Sc , rather than past the target and through the grids as in the conventional system. The gun has been placed to one side giving excellent screen visibility. When desired, normal electron-beam incidence can be achieved by rotation about axis $B-B$ which takes the target from position 3 to position 4.

The basic experimental requirements of INS are as follows:

(1) The incident ions must be slow in order to reduce the inherent energy broadening of the neutralization process. Data of the accuracy required can be obtained for ion energies K as low as 4 eV, as determined by the net acceleration in the lens system. Image-force attraction will increase this by about 2 eV. Thus we are working within a factor of 3 in energy or $\sqrt{3}$ in velocity of the absolute minimum possible if the ions were started toward the surface with infinitesimal velocity and were accelerated by the image force only. The ion optics, modes of lens operation, and negative feedback beam stabilization have been discussed elsewhere.^{19,21}

(2) The apparatus must have sufficiently high resolving power in the energy-distribution measurement. In the method used here of differentiating a retarding potential curve of electron current to electrode S , resolving power depends on the relative sizes of the target T and the electron-collecting sphere S . S is a sphere of 80-mm diameter (d_S) and T has a rectangular

²² J. J. Lander, J. Morrison, and F. Unterwald, Rev. Sci. Instr. **33**, 782 (1962).

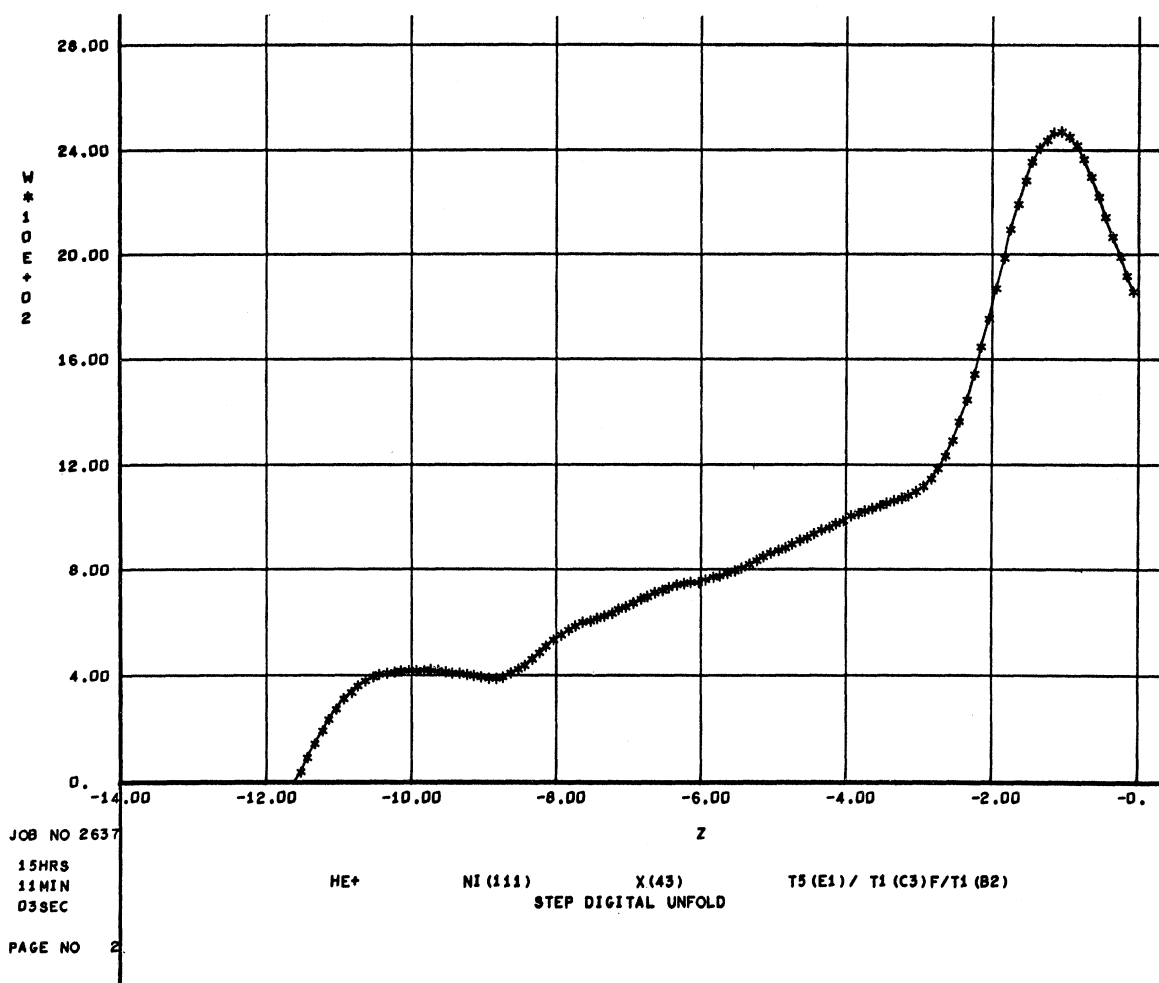


FIG. 11. Reproduction of the computer plot of the $U(z)$ function of Fig. 8 illustrating the quality of the digital data involved.

front face 14×7 mm which we may approximate by a sphere of 10-mm diameter (d_T). Monoenergetic electrons of energy E will be completely retarded from S in the V_{ST} interval between $[1 - (d_T/d_S)^2]E$ and E . Roughly, this corresponds to the convolution of a distribution in energy by an instrumental broadening function whose width at half-maximum is of order half the above retarding interval or $\frac{1}{2}(d_T/d_S)^2 E = 0.0075E$. At $E = 10$ eV this corresponds to an instrumental broadening of less than 0.1 eV.

(3) The data should have as little noise, particularly low-frequency noise (1–10 cps), as possible. Since we are dealing with ion beams of 10^{-9} – 10^{-10} A, and measure and differentiate electron currents to S which are as small as 10^{-13} A, this is a difficult requirement. High-frequency noise is effectively averaged out by counting during a 0.1-sec gating interval in the digitalization electronics. The traces of recorder plots of the analog derivatives in Figs. 1, 2, and 5 are representative of the best operating conditions. Electronic as well as digital

smoothing of the data or curve averaging is necessary, however.

(4) Very strict requirements must be met concerning the target-surface condition. If we are to determine bulk-state densities by INS the surface must be atomically clean and well ordered. We require background pressures in the apparatus below 10^{-10} Torr. Pressures as low as 6×10^{-11} Torr are consistently achieved. Low background gas pressure and low content of adsorbable impurities admitted with the noble gas used in the ion source make possible minimum monolayer adsorption times in the range 5–10 h. Flash-filament accumulation measurements indicate that we can sputter a target, anneal it, observe the LEED pattern, and complete the measurement of an $X_K(E)$ distribution before 2% of a monolayer of foreign gas has adsorbed on the target. More details concerning surface conditions and diagnostic methods will be given in subsequent publications of experimental results.

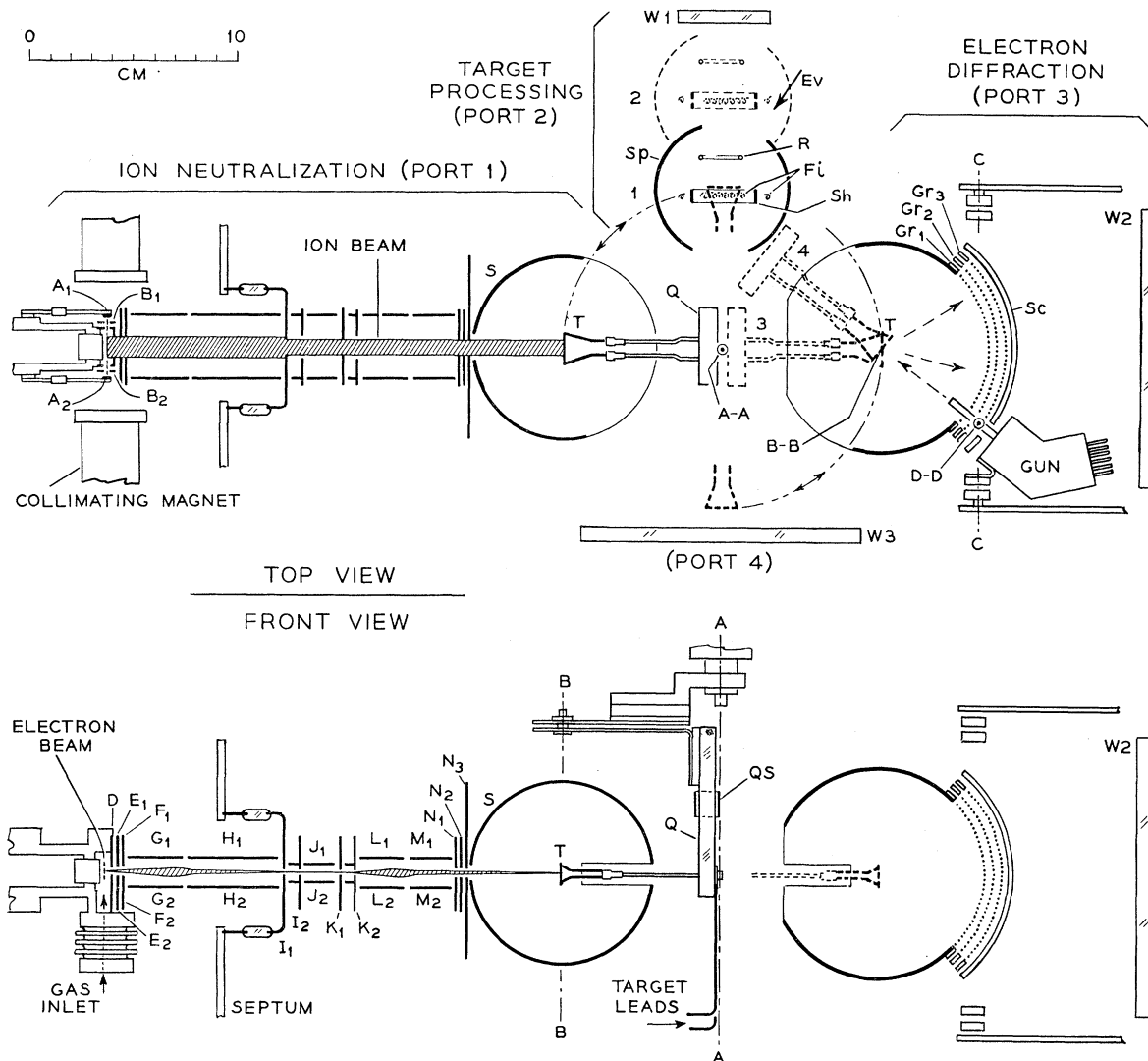


FIG. 12. Schematic top and front views of the experimental apparatus used.

V. THEORETICAL FEASIBILITY OF ION-NEUTRALIZATION SPECTROSCOPY

In the previous section on the experimental measurements we have indicated that it appears possible to meet the exacting standards required. Of course, the experimental measurements are intimately bound together with the procedures of data handling, and, as we shall see, the final judgment of the success of the experiment cannot be made until a feasible data-handling system has been devised. We are concerned here with the theoretical feasibility of the whole procedure of INS. It may be stated this way. Can each step of the data-handling procedure be made to work in a practicable manner and does it then produce a $U(\zeta)$ function for which we can give a reasonable physical interpretation in terms of bulk state densities, transition probability, and other factors?

There are really two aspects to the problem, the physical and the mathematical. Clearly these are interwoven; no physical result will be available for interpretation if it is not mathematically attainable. We proceed now to discuss the physics and mathematics of each of the basic steps of the data-handling procedure. These steps are

- (1) The debroadening extrapolation including the trimming of the high-energy tail (E near E_{\max} , ζ near 0). Steps (2) and (4) in Sec. III.
- (2) The division by $P(E)$. Step (3) in Sec. III.
- (3) The unfold of $F(\zeta)$ to produce $U(\zeta)$. Step (5) in Sec. III.

VI. THE DEBROADENING EXTRAPOLATION

As we shall see, the success of an electronic spectroscopy of solids based on the ion-neutralization process

requires that transition probability vary reasonably slowly with band energy ζ . This in turn requires a thin barrier between ion and solid with consequent relatively large transition rate and energy broadening. Initial-state lifetime broadening and nonadiabatic broadening due to the motion of the ion are the principal broadening components.³ Nonadiabatic broadening is appreciable even at the lowest ion velocities which are experimentally feasible and even, in fact, at the lowest possible "image-force velocity." Thus we expect to have to "debroaden" the measured $X_K(E)$ distributions. We are talking about an amount of broadening which varies with ion and solid but lies in the range 0.2 to 1 eV for 5-eV He⁺ ions.

In the forward model (Sec. II) broadening was introduced by convoluting the $F(\zeta)$ function with a symmetrical broadening function such as the Gaussian or the Lorentzian. Writing the unbroadened function generally as $Y_0(E)$ and the broadening function as $B(X)$, this convolution integral is

$$Y_1(E) = \int_{-\infty}^{\infty} B(X)Y_0(E-X)dX = B*F_0. \quad (15)$$

Our problem is to reverse this procedure at some point in the INS data handling and to determine the unknown Y_0 from the measured Y_1 . There is a considerable literature relating to the removal of instrumental broadening of spectral lines^{23,24} and x-ray diffraction lines,^{25,26} the effects of antenna smoothing in radio astronomy,²⁷ and the sharpening of observational data on the darkening of the solar limb.²⁸ In each of these cases, unlike our own case, the broadening function is independently known or can be determined. Van Cittert's first-order procedure²³ is then to convolute the known broadening function B with the measured Y_1 to obtain a function $Y_2 = B*Y_1$ and then to take $(Y_1 - Y_2)$ as a first-order approximation to $(Y_0 - Y_1)$. Thus he obtains

$$Y_0 = Y_1 + (Y_1 - Y_2) = 2Y_1 - B*Y_1. \quad (16)$$

Higher order approximations involving further successive convolutions of the experimental data have also been made.²⁴

Although it cannot be applied in our case because we do not know B , Van Cittert's approximation has been suggestive of the possibility of finding Y_0 from two measured distributions using the first of Eqs. (16) if a way of determining how Y_2 is to be measured relative to Y_1 can be found. In our case the Y functions are the $X_K(E)$ distributions which broaden as K is increased; so the problem could be stated thus: Having a dis-

tribution $X_{K_1}(E)$, at what K_2 shall another distribution be measured so that $X_0(E) - X_{K_1}(E) = X_{K_1}(E) - X_{K_2}(E)$? An equivalent way of stating the problem is embodied in Eq. (6) in terms of which our problem is to find the R parameter such that $(X_0 - X_{K_1}) = R(X_{K_1} - X_{K_2})$, X_{K_1} and X_{K_2} being any two measured distributions. We proceeded in Sec. III from Eq. (6) to Eq. (8) for $R_{K_1K_2}$ by use of the statement that $(X_0 - X_K)$ is proportional to ion velocity or \sqrt{K} . This dependence of broadening on ion velocity has been discussed elsewhere.³ The ion-velocity scale has been determined by making two corrections to the nominal ion accelerating voltage. Corrections are made (1) for the fact that the ions are formed in space at a potential in the bombarding electron beam which differs by 0.3 V from the potential of electrode D and (2) for the image force acceleration of the ion near the target surface. The increase in ion energy is related to the change in effective ionization energy near the surface.^{1,2} We have taken these to be equal and used $\Delta E_i = 2$ eV from the data fit of Ref. 2. This assumption suggests that the ion-solid separation at neutralization is about 2 Å, a not unreasonable value. Thus combining instrumental and image force corrections to V_{DT} we obtain for K ,

$$K = |V_{DT}| - 0.3 + 2 = |V_{DT}| + 1.7 \text{ eV}. \quad (17)$$

It should be pointed out that the result of this linear-extrapolation procedure is not the same as what one would obtain if the experiment could be performed of projecting the ion at lower and lower velocity toward the surface and could circumvent in some way the image force speedup near the surface. The results of such an experiment would drastically alter the form of $X_K(E)$ because as K decreases the ion-solid separation at neutralization increases, the barrier between ion and solid thickens, introducing a steep variation of transition probability with band energy ζ (Sec. VIII and Ref. 3). What the extrapolation procedure gives is approximately what one would measure could one produce ions of negligible velocity at the distance from the surface where the Auger process occurs for $K \sim 5$ –10 eV. The linear-extrapolation procedure should reduce the energy broadening to below 0.1 eV into the range of the instrumental broadening, at least near the top of the band.

(*Note added in proof.* The extrapolation procedure outlined above should take care of the broadening components which vary with ion velocity, but not final-state broadening, which is independent of ion velocity.³ Final-state broadening is zero at the top of the band and increases with increasing ζ deeper in the band. Recently we have experimented with extrapolations involving a variable R parameter which increases with increasing ζ . Results of this procedure will be discussed in later work. Extrapolation for constant R is used exclusively in this paper.)

In Fig. 5 we have seen an extrapolated $X_0(E)$ distribution for the cases of a metal showing a considerable

²³ P. H. Van Cittert, *Z. Physik* **69**, 298 (1931).

²⁴ H. C. Burger and P. H. van Cittert, *Z. Physik* **79**, 722 (1932).

²⁵ C. G. Shull, *Phys. Rev.* **70**, 679 (1946).

²⁶ M. S. Patterson, *Proc. Phys. Soc. (London)* **A63**, 477 (1950).

²⁷ R. N. Bracewell and J. A. Roberts, *Australian J. Phys.* **7**, 615 (1954).

²⁸ P. B. Fellgett and F. B. Schmeidler, *Monthly Notices Roy. Astron. Soc.* **112**, 445 (1952).

amount of broadening. We see that the linear-extrapolation procedure of Eq. (6) fails at the high-energy end of the distribution, producing negative values of $X_0(E)$. Thus we should not be surprised if the $F(\zeta)$ function derived from an $X_0(E)$ like that of Fig. 5 simply by throwing away the negative portions at higher E should prove to be unsatisfactory. In fact, as we shall see, such $F(\zeta)$ functions do not unfold properly. Further trimming of the function near the ordinate axis is required. As discussed in Sec. IX, this not only makes unfolding possible but brings the $F(\zeta)$ and $U(\zeta)$ functions into agreement with what is expected near the Fermi level from other considerations. Several ways of adjusting the data in this region could be used. In that employed almost exclusively to date, a new crossing point for the curve is chosen and the increment necessary to accomplish this is applied to the digital F values in linearly decreasing magnitude between this new zero of the F function and its first point of inflection. $F(\zeta)=0$ in any case defines $\zeta=0$.

Finally, in this section we mention the anomalous R values needed for Ne^+ ions. When the extrapolation methods discussed are applied to $X_K(E)$ distributions for Ne^+ it is immediately apparent, in comparison with extrapolation of He^+ data, that a much larger extrapolation has been effected. This is undoubtedly related to the anomalously large energy broadening found for Ne^+ .³ Ne^+ broadening, although linear with respect to v , was found to be considerably larger than that for He^+ , in violation of what one expects if broadening depended on ion velocity in going from one ion to another. Ar^+ broadening is considerably smaller than He^+ broadening, as expected. This behavior for Ne^+ is possibly related to another anomalous behavior of Ne^+ , namely, that of total electron yield with respect to ion velocity which was attributed to the involvement of excited states in the neon atom in the neutralization process. As discussed elsewhere,³ this could account for greater broadening in the velocity range where such excited states are involved. As ion velocity decreases, however, we expect the excited states to play a decreasing role and, in terminology used earlier,¹ to go from a mixture of Auger neutralization and Auger de-excitation to pure Auger neutralization. Thus a linear extrapolation of Ne^+ data to $v=0$ would overcorrect the data, as is found. Smaller R values are used for Ne which match the form of the high-energy end of $X_0(E)$ for Ne^+ to that for He^+ . This results in a good match for the $U(\zeta)$ curves as seen in Figs. 9 and 10.

VII. DIVISION BY ESCAPE PROBABILITY

The ion-neutralization process has two basic dependences on energy. One is the dependence on band energy ζ , and involves the density-of-initial-states and matrix-element factors which depend on the position of the participating electrons in the band. The second energy dependence is that on final-state energy which can be taken as E , the energy of the ejected electron. This

includes final-state density and escape probability of the excited electron. The function $P(E)$ is understood to include not only escape probability, but all other E dependences including final-state density. As can be seen in Fig. 4, structure traceable to an E dependence will remain stationary on the E scale whereas features arising from a ζ dependence will be shifted on the E scale for different ions by the difference in effective ionization energy [Eq. (2) and Fig. 2].

It is clear that a relatively smooth $P(E)$ function such as that of Eq. (10), shown plotted in Figs. 4, 7, 8, cannot account for sharp peaks or variations in the density of final states. On comparing He^+ , Ne^+ , and Ar^+ results we have not seen any effects which appear to result from features in the density of final states. From results to date it appears that a common $F(\zeta)$ and a common $P(E)$ function may be found for different ions for the same solid. It can be shown that the existence of either a common $F(\zeta)$ or a common $P(E)$ function requires the existence of the other.

VIII. PHYSICAL JUSTIFICATION OF UNFOLDING AND THE MEANING OF $U(\zeta)$

Having arrived at an $F(\zeta)$ function characteristic of the ion-neutralization process for a given solid but essentially independent of the specific ion used, we can proceed only if $F(\zeta)$ is expressible as a convolution square or self-fold of a function $U(\zeta)$ as given in Eq. (3). Our problem in this section is to discuss how nearly Eq. (3) expresses the physics of the situation and what the $U(\zeta)$ function then means. We shall not repeat the more general theoretical setup of the problem to be found in Secs. XI–XV of Ref. 2, but shall introduce only those elements necessary to our purposes here.

As in Ref. 2 we assume initially that the process can be described with reasonable accuracy in the one-electron approximation. We shall find that we obtain a very reasonable explanation of the INS results for Cu and Ni on this basis. This appears to indicate that final-state interactions and many-body effects do not play a dominant role in the work we have done to date. This does not preclude finding such effects in the INS results as more detailed comparisons with SXS and PES are made. The effects to be expected from some possible final-state and many-body interactions are mentioned later in this section.

The elemental transition rate for a pair of electronic transitions such as are depicted in Fig. 3 depends on band energies of the two electrons, angles, and ion-solid separation. We may write it as

$$r_i(\zeta, \Delta, \Omega, s) = (2\pi/\hbar) |H_{fi}|^2 N_f(E) d\Omega, \quad (18)$$

using standard, time-dependent perturbation theory. In Eq. (18) Ω is the solid angle, H_{fi} the matrix element, and $N_f(E)$ the density of final states. Since we are interested in the totality of those elemental processes which produce excited electrons in dE at E , we must integrate r_i over angle, ion-solid separation s , and the

energy difference Δ (Fig. 3). This gives us the function $F(\zeta)$ which may be written

$$F(\zeta) \propto \int_0^{\zeta} |H_{fi}|^2 N_V(\zeta + \Delta) N_V(\zeta - \Delta) d\Delta, \quad (19)$$

for constant density of final states. Taking account of antisymmetrization of the total wave functions including space and spin functions, $|H_{fi}|^2$ may be written as

$$|H_{fi}|^2 = [H'^2 + H''^2 - H'H''], \quad (20)$$

in terms of the "elemental" matrix elements H' and H'' for each of the elemental pairs of transitions shown in Fig. 3.² H' may be written as

$$H' = \int \int u_o^*(1) u_o^*(2) (e^2/r_{12}) u_v''(1) u_v''(2) d\tau_1 d\tau_2, \quad (21)$$

in terms of wave functions shown in Fig. 13. H'' is obtained from Eq. (21) by interchanging electrons 1 and 2 in the initial-state wave functions as dictated by Fig. 3.

As discussed in Sec. XII of Ref. 2, we can distinguish two general kinds of matrix-element dependence. One arises from exchange-matrix-element cancellation and is a dependence on the energy difference 2Δ between the participating electrons. The other is the dependence on ζ_1 and ζ_2 of the participating electrons. We note that the matrix element may be viewed as a Coulomb interaction integral between two charge clouds $u_o^*(1)u_v''(1)$ and $u_o^*(2)u_v''(2)$ for electrons 1 and 2, respectively. This is seen if we rewrite Eq. (21) in the form

$$H' = \int \int u_o^*(1) u_v''(1) (e^2/r_{12}) u_o^*(2) u_v''(2) d\tau_1 d\tau_2. \quad (22)$$

The Coulomb-interaction term most likely does not have the simple form written here. H' will be larger the larger the magnitudes of the component wave function products for each electron and the larger their overlap.

If we write²

$$H'' = mH', \quad 0 \leq m \leq 1, \quad (23)$$

Eq. (20) becomes

$$|H_{fi}|^2 = H'^2 [1 + m + m^2] = H'^2 [\frac{3}{4} + (m - \frac{1}{2})^2]. \quad (24)$$

Thus near the edges of bands or in narrow bands the two electrons lie at nearly the same energy and $m \sim 1$. The greatest deviation of $|H_{fi}|^2$ from H'^2 occurs at $m = \frac{1}{2}$ when $|H_{fi}|^2 = \frac{3}{4}H'^2$. m clearly must be a function of the energy separation of the two electrons in the band, 2Δ . Electron exchange changes the wave-function products from the pair $u_o^*(1)u_v''(1), u_o^*(2)u_v''(2)$ to the pair $u_o^*(1)u_v''(2), u_o^*(2)u_v''(1)$. The changes in the product wave functions tend to compensate in the overlap region. Thus if the range of interaction between the participating electrons is small, we expect little effect of electron exchange. Since, as we shall see, there are reasons for believing that this is approximately the

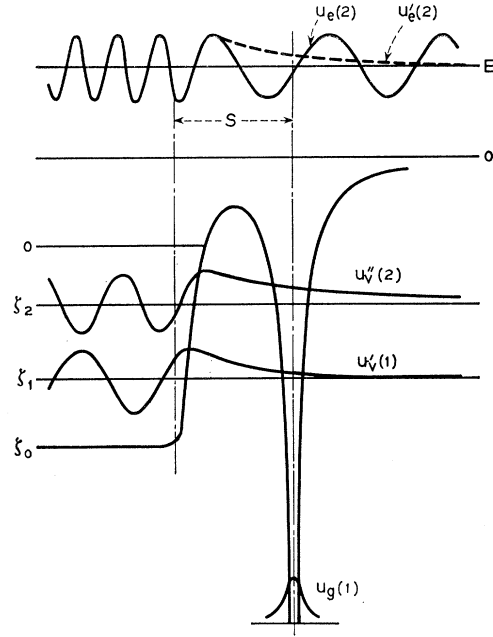


FIG. 13. Electron-energy diagram showing electron wave functions for the initial band states, $u_v'(1)$, $u_v''(2)$, for the atomic ground state, $u_o(1)$, and for two excited states, one which crosses the surface barrier, $u_e(2)$, and another which is internally reflected there, $u_e'(2)$.

case, we shall neglect the effects of electron exchange and any possible dependence on energy difference of the two electrons.

We are now left with the matrix element dependences on ζ_1 and ζ_2 . The nature of these dependences involves two fundamental characteristics of the neutralization process: (1) the thickness of the barrier between ion and solid when transition occurs, and (2) the range of the interaction between electrons 1 and 2. As discussed elsewhere,³ a thick barrier would limit the tunneling of electron 1 to ζ_1 values near zero at the top of the band. This would put us at what we have called the one-electron limit of the problem since ζ_2 only would then be allowed to vary through the band. This would mean that the $F(\zeta)$ function and not the $U(\zeta)$ function of Figs. 7 and 8 would be related to the state density in the filled band. From what we know of the transition metals Cu and Ni this is clearly impossible. The expected d bands show up in $U(\zeta)$, not $F(\zeta)$. Furthermore, when the $U(\zeta)$ functions are plotted on the same plot as in Fig. 14 it appears that both the d band and the background of $s-p$ electrons under the d bands decrease in magnitude with increasing ζ rather than remaining approximately constant as band calculations require. This points to a relatively weak tunneling dependence on band energy and is further evidence that we are near the two-electron or Auger limit of the process.

We are now in a position to summarize the transition probability factors for electron 1 of Fig. 13, the "down" electron. These factors are those which affect the mag-

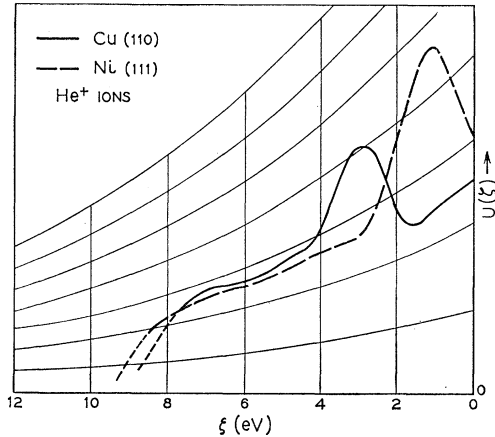


FIG. 14. Plots of the unfold functions $U(\xi)$ from Figs. 7 and 8 for Cu(110) and Ni(111). The constant ordinate lines are plots of the exponential $A \exp(-0.12\xi)$.

nitude of the wave-function product $u_g^*(1)u_v'(1)$. Since $u_g^*(1)$ is restricted to the region of the atom by the rapid fall-off of $u_g^*(1)$ away from the atom, this wave-function product is governed by the tunneling efficiency of $u_v'(1)$ into the atomic well. This in turn depends on ξ_1 , on the symmetry character of the band wave function which we designate by l_1 , and on the angle θ_1 which the electron's \mathbf{k} vector makes with the surface normal. We shall write the transition probability factor as $q_1(\xi_1, l_1, \theta_1)$ and the probability that an electron in $d\xi_1$ at ξ_1 becomes a "down" electron in a neutralization process as the product $q_1(\xi_1, l_1, \theta_1)N_V(\xi_1)$.

The magnitude of $u_v'(1)$ at the position of the atom is governed by an expression of the form

$$q_1(\xi_1, l_1, \theta_1) = f(l_1) \times \exp\left(-\left\{ (2m)^{1/2} \hbar \left[(\xi_0 + \varphi) - (\xi_0 - \xi_1) \cos^2 \theta_1 \right]^{1/2} \xi_1 \right\}\right), \quad (25)$$

in which the dependence on symmetry is given by $f(l_1)$ and the dependence on ξ_1 and θ_1 by the exponential. ξ_0 is defined in Figs. 3 and 13. The term $(\xi_0 + \varphi)$ is total barrier height and $(\xi_0 - \xi_1) \cos^2 \theta_1$ is proportional to $\hbar v_n^2$, the energy associated with velocity normal to the surface. $f(l_1)$ expresses the fact that the magnitude outside the solid of the atomic orbital at a given distance from the nucleus of a surface atom decreases in magnitude as l_1 increases, i.e., as one goes from an s electron to a p , to a d , etc. (Sec. XII of Ref. 2). This effect is to be seen in the results for the d electrons in Cu and Ni (Fig. 14), where the magnitude of the d peak is much reduced relative to the s - p background (Sec. XI). An attempt to measure areas of the d peak and the s - p background indicates that the d peak is reduced in relative magnitude in both Cu and Ni by several times a factor of 10. The ratio of d -peak height to s -electron intensity near the Fermi level for Cu in Fig. 14 is about a factor of 10 lower than this ratio for the PES results.¹² The exponential factor is what one expects for a plane wave incident on a barrier at which it is totally reflected.

It indicates a decrease in q_1 with increasing ξ_1 and θ_1 , favoring electrons near the top of the band and those which are moving normally to the surface. The dependence on θ_1 might be different for d electrons from what it is for s or p since the d electrons are not as well approximated by plane waves. We have seen evidence for the ξ_1 dependence in Fig. 14. Propst²⁹ has attempted a calculation of this tunneling factor and for a reasonable choice of s has obtained $\exp(-0.4\xi)$, a somewhat steeper exponential than that in Fig. 14. Possible reasons for this are discussed in Sec. IX.

Turning now to the transition probability factor $q_2(\xi_2, l_2, \theta_2)$ for the "up" electron, electron 2 of Fig. 13, we are confronted with the second fundamental characteristic of the neutralization process, namely, the range of interaction between electrons 1 and 2. If electron 2 could be excited over large distances from electron 1, the $u_e^*(2)u_v''(2)$ product would be dominated by the bulk parts of the wave functions and q_2 could hardly be expected to have the same dependences as q_1 . Under these circumstances we write $|H_{f_i}|^2$ in Eq. (19) as the product $q_1 q_2$ and obtain

$$F(\xi) \propto \int_0^\xi q_1(\xi + \Delta, l_1, \theta_1) N_V(\xi + \Delta) \times q_2(\xi - \Delta, l_2, \theta_2) N_V(\xi - \Delta) d\Delta. \quad (26)$$

This is Eq. (4) with $U_1 = q_1 N_V$ and $U_2 = q_2 N_V$. If on the other hand the perturbation in Eq. (21) limits r_{12} to small values, the important part of $u_e^*(2)u_v''(2)$ is also that part which overlaps the region of the atomic well and $q_1 \sim q_2$. Under these circumstances the unfolding of Eq. (3) in the INS procedure is justified. In an intermediate case, unfolding of Eq. (3) for q_1 different but not greatly different from q_2 would yield a sort of average $U(\xi)$ which would still be interpretable.

There is evidence that electron 2 is excited near the surface and hence near electron 1. This comes from the experimental result that the ion-neutralization distributions have many, many times fewer inelastically scattered secondary electrons than would the one-electron photoelectric emission process for $\hbar\nu \cong 18$ eV which is the equivalent of the He^+ ion-neutralization process. Thus electron 2 must be excited much closer to the surface than are photoelectrons in these experiments.^{12,13} In a metal we would expect the screening of the Coulomb term in Eq. (21) to limit r_{12} to ~ 0.5 Å were it not for the large energy transitions which lie above the plasma frequency. If one considers the neutralization process to be the release of a photon by the "down" electron which is absorbed by the "up" electron we point out that this photon is not a plane-wave photon as in the photoelectric effect. The dipole which generates the radiation lies very close to the solid. Thus other band electrons at the surface of the solid lie in the near-field region of the dipole radiation which falls off very rapidly with distance and limits excitation of electron 2 to the

²⁹ F. M. Propst, Phys. Rev. **129**, 7 (1963).

surface of the solid. Heine³⁰ has shown that the long range of the unscreened potential does not lead to any divergences which might be expected in calculating the emergent current. Since only those elemental processes which correspond to large momentum change contribute effectively, Heine concludes that the excited or "up" electron originates largely in the first atomic layer and outside the solid. He also has discussed the momentum dependences of the transition probability.

Finally, we note that the results of unfolding Eq. (3) produce very reasonable results in terms of the known transition probability factors. Since it is improbable that the transition probability factors for the up and down electrons are identical, we conclude that the unfolding produces a reasonable $U(\zeta)$ average between the true $U_1(\zeta)$ and $U_2(\zeta)$. Under these circumstances we expect the $U(\zeta)$ obtained from the unfold of Eq. (3) to display the dependences on ζ , l , and θ which are like those deduced for q_1 for the down electron only. This is, in fact, the case.

The one-electron approximation used here in discussing the physics of INS does not, as said earlier, include exciton-like, final-state interactions or many-body effects of possible importance. An example of a final-state interaction is that between the two holes formed in the valence band. By virtue of screening we would expect the energy involved to be appreciable only if the two holes were formed on the same atom. The potential energy of repulsion eventually appears as kinetic energy of the holes which decreases the energy available for excitation of the up electron. A distribution in magnitude of such repulsive energies would result in a broadening of the observed d band in copper, for example. Integration of this effect over the volume in which excitation of the up electron is appreciable would greatly reduce the probability of very close initial proximity of the two holes even if the interaction radius were as small as twice the lattice constant. Other interactions of a many-body nature could involve excitation of more than one up electron or simultaneous excitation of an electron and a plasmon. There is no direct evidence for the first of these in results to date. The second would essentially remove the up electron from observation because of the large value of the plasmon energy in the materials studied so far. As said elsewhere, we take the position that the one-electron approximation gives a reasonable first interpretation of the results, there being no direct evidence as yet of important final-state or many-body interactions. Some further discussion of many-body effects is included in Sec. XI, (1).

IX. THE MATHEMATICS OF UNFOLDING

We discuss in this section the means of unfolding the integral expression of Eq. (3) to obtain the function

TABLE I. Analytic fold and unfold functions which are solutions of $F(\zeta) = \int_0^\zeta U(\zeta + \Delta)U(\zeta - \Delta)d\Delta$.

	$U(\zeta)$	$F(\zeta)$
(1)	A	$A^2\zeta$
(2)	$A\zeta$	$\frac{2}{3}A^2\zeta^3$
(3)	$A\zeta^{1/2}$	$\frac{1}{4}\pi A^2\zeta^2$
(4)	$A\zeta^{-1/2}$	$\frac{1}{2}\pi A^2$
(5)	$A+B\zeta$	$A^2\zeta + 2AB\zeta^2 + \frac{2}{3}B^2\zeta^3$

$U(\zeta)$. Given Eq. (3),

$$F(\zeta) = \int_0^\zeta U(\zeta + \Delta)U(\zeta - \Delta)d\Delta, \quad (3)$$

we can readily write down some analytic functions satisfying this relation. Several examples are given in Table I. Also, as indicated in Sec. III, we can produce the digital fold-unfold relations of Eqs. (13) and (14) by assuming $U(\zeta)$ to be approximated by a step function, i.e., $U(\zeta)$ constant at the value U_{2m-1} in the interval $(2m-2)\Delta\zeta \leq \zeta \leq 2m\Delta\zeta$. [See Eq. (12).] The relations of Eqs. (13) may be obtained from a matrix in which the term in the m th row and the p th column is $U_{2m-1}U_{2p-1}$. F_n is the sum of terms appearing along the diagonal of the matrix running from the $U_{2n-1}U_1$ term to the U_1U_{2n-1} term. This gives the F_n of Eqs. (13). Sequential unfold by Eqs. (14) proceeds through the matrix from the U_1^2 term in the upper-left-hand corner.

Unfolding by means of the step-digital-unfold relations of Eqs. (14) is fraught with difficulties, and considerable time and effort were expended in overcoming these. Only after we had come to an understanding of the basic instabilities and error introductions of the method was it possible to apply Eqs. (14) successfully. During this work several different unfolding methods were tried. These are mentioned briefly later in this section.

The step-digital-unfold sequence of Eqs. (14) displays two basic instabilities. The first of these, which we call the $\Delta 2$ instability, arises for the case $F(\zeta) = 0$ at $\zeta = 0$ when $d^2F/d\zeta^2$ or the second difference $\Delta 2$ is too large. The step-digital fold-unfold relations of Eqs. (13) and (14) are completely accurate only for the case $F(\zeta) = \zeta(d^2F/d\zeta^2 = 0)$, which is entry (1) in Table I. Digitalization of $F(\zeta) = \zeta$ unfolds properly, giving the digitalized form of $U(\zeta) = 1$, as is seen in Fig. 15(a). When one digitalizes $F(\zeta) = \frac{2}{3}\zeta^3$ [entry (2) in Table I], however, and tries to unfold this by Eqs. (14) one is in serious trouble in a few points, as Fig. 15(b) indicates. $F(\zeta)$ in this case starts out with zero slope, greatly different from the case $F(\zeta) = \zeta$, $\Delta 2 = 0$ for which Eqs. (14) are accurate. Note that the digitalization of $F(\zeta) = \frac{2}{3}\zeta^3$ was done to 8-place accuracy. Thus no matter how accurate one's digital data for $F(\zeta)$, one is in trouble if $F(\zeta) = 0$ at $\zeta = 0$, $dF/d\zeta$ is small, and $d^2F/d\zeta^2$ large. One can circumvent this difficulty by replacing the first 10 points of $F(\zeta)$ by the digitalized fold by Eqs. (13) of an assumed analytic fold $U(\zeta)$ and carefully matching this to the experimental data at the 11th point. In

³⁰ V. Heine, Phys. Rev. (to be published).

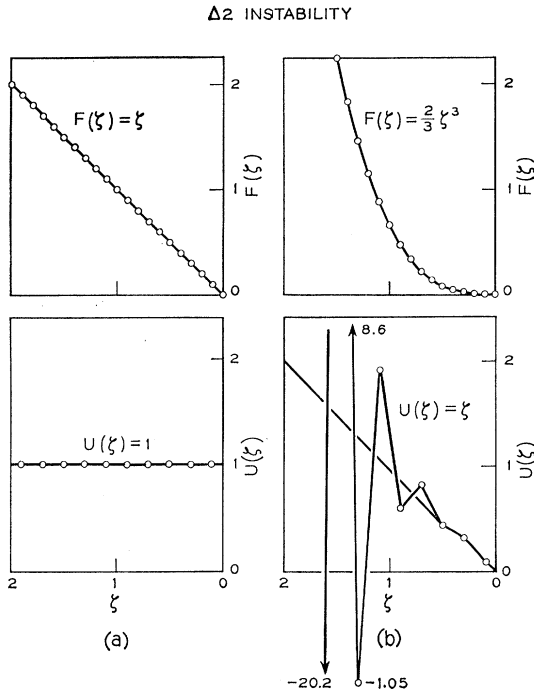


FIG. 15. $F(\zeta)$ and $U(\zeta)$ functions indicating (a) the absence, and (b) the presence of an instability caused by too large a second difference in the digital data at the onset of the $F(\zeta)$ function.

this way we were able to circumvent the $\Delta 2$ instability for some germanium data. We were then plagued, however, with the harmonic-error introduction discussed below.

The second instability of Eqs. (14) is a noise instability. If too much noise is allowed to remain in the data, the digital U_{2n-1} points will be alternately above and below the smooth $U(\zeta)$ function at distances which eventually increase to a very large value. This instability can be of point-to-point character or can involve longer ripples in the data which are not unlike the harmonics discussed below. The amount of smoothing used has been entirely adequate to circumvent this difficulty.

The unfolding procedure is found to be very sensitive to the form of the function $F(\zeta)$ near $\zeta=0$. This is believed to result from the convoluted nature of $F(\zeta)$. The value of $F(\zeta_1)$ at ζ_1 depends on the values of $U(\zeta)$ at all $\zeta < \zeta_1$. The initial portions of $U(\zeta)$ are used over and over again in developing $F(\zeta)$. Thus the onset portion of an experimentally derived $F(\zeta)$ near $\zeta=0$ must be consistent with the rest of the $F(\zeta)$ function if we are to unfold it to produce the correct unfold $U(\zeta)$. An "incorrect" initial portion of $F(\zeta)$ introduces error into $U(\zeta)$ in the form of harmonics whose magnitude and phase depend on relatively small changes in the initial portions of $F(\zeta)$. We have seen above that it is just here that we know least about $F(\zeta)$ by virtue of energy broadening and the failure of the linear extrapolation near $\zeta=0$. Figure 16 for Ni data illustrates this har-

monic-error introduction. If for $F(\zeta)$ we use a curve derived from an $X_5(E)$ distribution only and simply cut it off at $\zeta=0$ as shown at *a* in the inset of Fig. 16, the dashed curve for $U(\zeta)$ is obtained. If for $F(\zeta)$ we use an $X_0(E)$ curve like that of Fig. 5, discarding the negative portions, we have the $F(\zeta)$ shown at *b* in the inset of Fig. 16 and obtain the solid curve for $U(\zeta)$. Note the shift in phase of the spurious harmonic. When $F(\zeta)$ is cut off to the curve shown at *c* in the inset, curve 1 of Fig. 17 results. This curve no longer includes a spurious harmonic. Continuation of this trimming procedure by moving $\zeta=0$ toward larger ζ by 0.1-eV steps, distributing the incremental changes necessary to do this linearly over the succeeding data points with the increment reaching zero at the first point of inflection of the function, the series of curves 1-5 of Fig. 17 results. Notice that $U(\zeta)$ has now stabilized without harmonic-error introduction except for the changes brought about by the differing treatments of the data near $\zeta=0$. A further comment on the genesis of harmonic error is made below.

The above illustrates a basic characteristic of the ion-neutralization spectroscopy. Within the range of stable unfolding we cannot *a priori* choose among the curves of Fig. 17. However, we are quite sure that the "correct" $U(\zeta)$ function is to be found among those for which a stable unfold without harmonic introduction is possible. In fact, this necessity of making the initial portion of $F(\zeta)$ consistent with the rest of the function so that the stable unfold is possible considerably narrows the range of possible $U(\zeta)$ functions. However, it is necessary to choose among the stable solutions for $U(\zeta)$ such as those of Fig. 17, making use of other band-

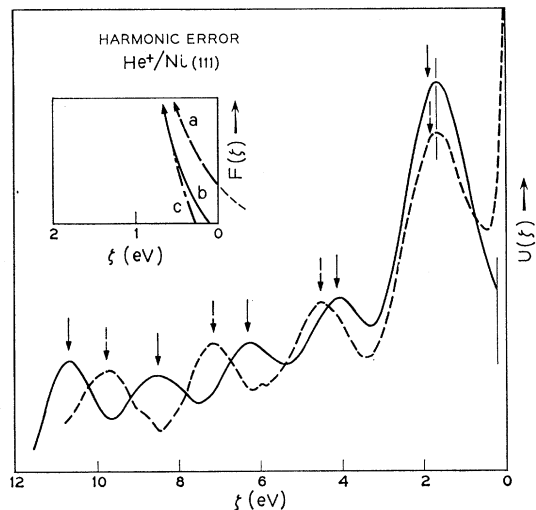


FIG. 16. $U(\zeta)$ functions illustrating change in harmonic error introduction when the initial portion of the $F(\zeta)$ function is varied. Curves *a* and *b* in the inset show the initial portions of the $F(\zeta)$ functions corresponding to the dashed and full $U(\zeta)$ curves, respectively. Curve *c* of the inset corresponds to curve 1 of Fig. 17, as indicated in the text.

structure information in this choice, as will be explained in more detailed publications for individual solids. This procedure gives us an answer which could misplace structure observed deeper in the band by no more than a few tenths of a volt. INS more accurately locates deeper lying structure features relative to each other than to the Fermi level.

During the above studies of the step-digital-unfold procedure other methods of unfolding were investigated. Blackman³¹ pointed out that Eq. (3) had a simple electrical-network analog. A four-terminal network to whose input terminals a unit impulse (δ function at $t=0$) is applied produces the so-called unit impulse response function R_1 at its output terminals. This can be fed into a second identical network to obtain the unit impulse response function R_2 of two identical networks in tandem. R_1 is $U(\zeta)$ and R_2 is $F(\zeta)$ of Eq. (3). It was possible to set up a network on an analog computer and to display $U(\zeta)$ and $F(\zeta)$ on alternate cycles.³² Variation of the network parameters varied both $U(\zeta)$ and $F(\zeta)$. In principle, one could fit $F(\zeta)$ to a function determined in the ion-neutralization experiment and obtain $U(\zeta)$ in this way by trial and error.

Another possibility involves expansion of the unknown $U(\zeta)$ in terms of orthonormal functions and determination of the expansion coefficients from the given $F(\zeta)$. An analytic expression or a means of calculating digital F_n values from an assumed $U(\zeta)$ in terms of the expansion coefficient is then set up. The initially chosen coefficients are refined by a successive approximation program using least-squares fit of the calculated F_n to the experimental F_n . Two methods of doing this were investigated.

We expand the unknown $U(\zeta)$ in terms of orthonormal polynomials, writing

$$U(\zeta) = \sum_{n=0,t} a_n P_n(\zeta). \quad (27)$$

$F(\zeta)$ from Eq. (3) then becomes

$$F(\zeta) = \sum_{m,n=0,t} a_m a_n \int_0^\zeta P_m(\zeta-\Delta) P_n(\zeta+\Delta) d\Delta. \quad (28)$$

For $P_n(\zeta)$ we chose the shifted Chebyshev polynomials. It was soon found, however, that the procedure was impractical for two reasons. First, derivation of the polynomial expressions for the integral fold of the $P_n(\zeta)$ polynomials required in Eq. (28) was prohibitively tedious if carried to sufficiently high-order polynomials. Second, evaluation of the integral in polynomial form had prohibitively large round-off errors since the final value, of order unity, was obtained as the result of subtracting very large numbers.

Another scheme based on Eq. (27) was then tried and used successfully. From an initial choice of the a_n , the function $U(\zeta)$ was evaluated at 120 points by Eq.

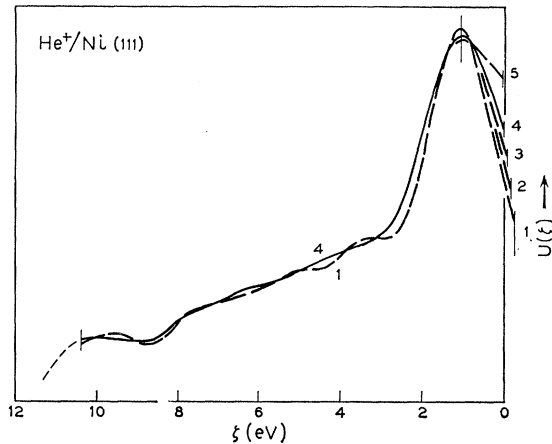


Fig. 17. $U(\zeta)$ functions for He^+ ions on Ni(111) illustrating the effect of trimming the initial portion of the $F(\zeta)$ function. All these curves are in the range where harmonic error has been depressed.

(27). These U_n data were then folded by Eqs. (13) to obtain F_n . A subset of F_n was then compared with the experimental values and a least-squares error calculated. Minimization of this least-squares error was carried out using a successive-approximation program.³³ Although tedious to apply, the program worked if one had a reasonable initial choice of $U(\zeta)$. Although the program was not used extensively, enough was done with it to show that harmonic error was also introduced here if the initial portion of $F(\zeta)$ was "incorrect."

The setup of the successive-approximation method illuminates the question of harmonic-error introduction in a way worth mentioning. The a_n coefficients of Eq. (27) may be divided into two classes: those to which the least-squares error is sensitive and those to which it is not. If the least-squares error is insensitive to a given a_n , it means that a large amount of this harmonic can be inserted into the $U(\zeta)$ function without greatly affecting the resultant $F(\zeta)$. The harmonic in $U(\zeta)$ "folds itself out," so to speak, in producing $F(\zeta)$. Conversely small "errors" in the experimental $F(\zeta)$ can demand large harmonic amplitude of such an insensitive harmonic as our experimentation with the initial portion of $F(\zeta)$ has shown. Methods of preventing the introduction of these "insensitive" harmonics have been tried. An iterative procedure based on repetitive application of Eqs. (14) and involving reduced weight on points at higher ζ was tried with the hope of stopping the procedure before "insensitive" harmonics developed. The method was only partially successful.

The only really practicable unfolding of the experimental data uses the step-digital-unfold relations and has proceeded by cutting off the initial portions of $F(\zeta)$ step by step until harmonic-error introduction was depressed and a stable solution insensitive to further cutting of the initial portion was achieved. The

³¹ R. B. Blackman (private communication).

³² This was done at the kind instigation of C. F. Simone.

³³ C. L. Semmelman and J. M. Schilling (unpublished).

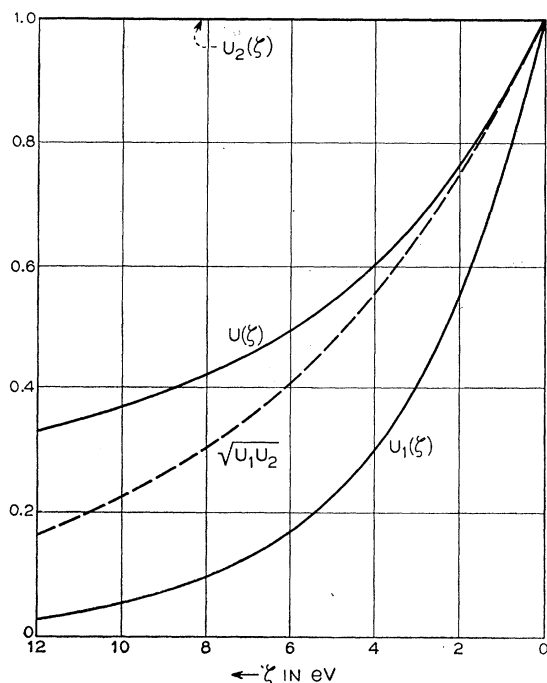


FIG. 18. Functions illustrating the averaging effect produced by unfolding according to Eq. (3) when Eq. (4) really applies. $U(\zeta)$ is the unfold by Eq. (3) of the fold of $U_1(\zeta) = \exp(-0.3\zeta)$ and $U_2(\zeta) = 1$ by Eq. (4).

unfold procedure of Eqs. (14) has been used independently by McMillan,³⁴ who has encountered Eq. (3) in the study of superconducting tunneling. Here the analytic F and U functions are like those of entry (4) in Table II and no unstabilities or harmonic-error introduction has been encountered in the digital-unfolding procedure. Apparently a sharp step in $F(\zeta)$ at $\zeta=0$ facilitates unfolding, a fact which encouraged the procedure used here of cutting off the tail of $F(\zeta)$ at $\zeta=0$.

Trimming the $F(\zeta)$ function to a steeper initial slope requires a larger initial rise in $U(\zeta)$ at $\zeta=0$. For metals this is what is expected physically. The transition probability favors involvement of electrons near $\zeta=0$, again giving rise to a sharp step at the top of the band. This latter effect apparently accounts for the results for semiconductors where a rather steep rise of $F(\zeta)$ at $\zeta=0$ is also required for proper unfolding.

Finally, in this section we discuss the mathematical effect of unfolding an $F(\zeta)$ function to get a $U(\zeta)$ function by Eq. (3) when different transition probabilities for the up and down electrons would indicate that Eq. (4) applies. In this case we would expect the $U(\zeta)$ function from unfolding Eq. (3) to be some sort of average between the $U_1(\zeta)$ and $U_2(\zeta)$ function of Eq. (4). The nature of this averaging is best illustrated by an example. The functions $U_1(\zeta) = \exp(-0.3\zeta)$

and $U_2(\zeta) = 1$, shown in Fig. 18 were folded by Eq. (4). The fold thus produced was then unfolded by Eq. (3) and the $U(\zeta)$ function of Fig. 18 obtained. For comparison the geometric mean of the original U_1 and U_2 is also plotted. Thus we see that if $U_1 \neq U_2$ we expect our unfold to show a smaller variation with ζ than that of $U_1(\zeta)$, which by the discussion of Sec. VIII should be that of the down electron. We would not expect the position of local band-structure features to be affected by this averaging, however. Perhaps it is averaging of this sort which accounts for the fact that the exponential $[\exp(-0.12\zeta)]$ appropriate to the s - p electrons in Fig. 14 is less steep than the exponential $[\exp(-0.4\zeta)]$ calculated by Propst²⁹ (Sec. VIII). Propst considered that only the down electron tunnels into the atomic well with the up electron being excited deeper in the solid.

X. ION-NEUTRALIZATION SPECTROSCOPY IN THE PRESENCE OF ORDERED SURFACE MONOLAYERS INVOLVING FOREIGN ATOMS

The claim has been made that although the surface character of the ion-neutralization process affects transition probability factors in the transition density, the density-of-states factor for atomically clean surfaces is that of the bulk solid except for the two modifications for semiconductors. We turn now to discuss briefly the effect of foreign surface atoms on INS. A preliminary report concerning this has been made, but it did not include unfolding of the energy distributions.³⁵ We limit ourselves here to surfaces in which atoms from the bulk and foreign atoms form a crystallographically ordered monolayer surface phase, the surface of type b mentioned in the Introduction. An example is the centered (2×2) nickel-oxygen structure, studied by

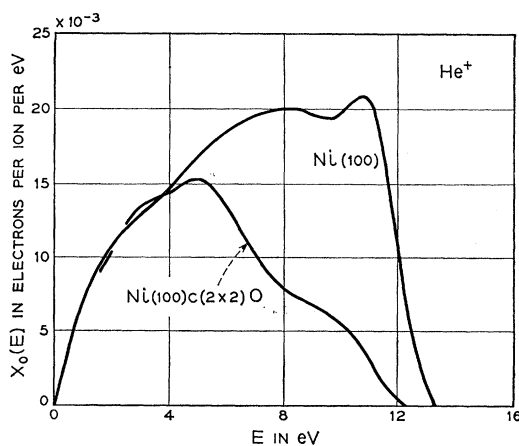


FIG. 19. $X_0(E)$ distributions for He^+ ions incident on an atomically clean (100) face of Ni and a (100) face on which a centered (2×2) surface two-dimensional crystal of Ni and O has been grown.

³⁴ W. L. McMillan and J. M. Rowell, Phys. Rev. Letters 14, 108 (1965); and private communication.

³⁵ H. D. Hagstrum, Y. Takeishi, G. E. Becker, and D. D. Pretzer, Surface Sci. 2, 26 (1964).

Mac Rae,³⁶ which forms on Ni when exposed to oxygen. Experimentally it is found that the presence of this two-dimensional surface lattice modifies the electron energy distribution $X(E)$ drastically. This is shown in Fig. 19, where $X_0(E)$ distributions are shown for atomically clean Ni and for Ni with the $c(2 \times 2)$ ordered phase of nickel and oxygen on the surface. Figure 19 shows that for the surface containing oxygen there are far fewer of the faster electrons than for the atomically clean surface. The two-dimensional surface crystal produces a density of states throughout the combined crystal lattice which differs from that of the crystal having a clean surface. This difference is small, however, since there are about 10^{15} surface atoms on one face of a centimeter cube containing about 10^{22} atoms, and it will elude detection by any method like SXS or PES, which samples an appreciable region of the bulk.

The surface crystal will act like a band-pass filter for wave functions from the bulk crystal to which it is attached. It will act as a forbidden region in some energy ranges and will permit large wave-function magnitude in others. Because INS samples surface-wave-function magnitude we expect to be able to determine, and results to date confirm that we can, this band-structure feature of the surface-monolayer crystal. We would expect, *a priori*, that we can do this uniquely only if we are willing to make an assumption as to where the up electron is excited. If it arises in the surface monolayer then $F(\zeta)$ is represented by the convolution square of Eq. (3) which can be unfolded. This leads, for the $X_0(E)$ distribution of Fig. 19, to the $U(\zeta)$ for Ni(100) $c(2 \times 2)$ O in Fig. 20. The $U(\zeta)$ for the atomically clean Ni(100) surface is also shown in Fig. 20. $U(\zeta)$ for Ni(100) $c(2 \times 2)$ O differs markedly and interestingly from $U(\zeta)$ for the clean surface. We note the appearance of a broad band lying at energies $3.5 < \zeta < 7.5$ eV, which on the assumption made is the band in which the surface crystal transmits the bulk wave functions. We note also the decrease in intensity of the bulk d band near the Fermi level. Wave functions in this band must tunnel through a forbidden region in the surface crystal and are, as a result, much decreased in intensity at the ion position.

If we go to the other extreme and assume that the up electron arises in the bulk of the crystal the appropriate expression for $F(\zeta)$ is the convolution product of Eq. (4) in which $U_1(\zeta)$ characterizes the down electron and $U_2(\zeta)$ should be a bulk function something like the $U(\zeta)$ function for clean Ni(100). We have very recently shown that unfolding the convolution product using the $U(\zeta)$ for clean Ni(100) as $U_2(\zeta)$ produces essentially the same low-lying features in $U_1(\zeta)$ as was found in $U(\zeta)$ from the convolution product. These results will be discussed in detail elsewhere. INS is also sensitive to amorphously held gas on the surface, as has been amply demonstrated in earlier work.^{37,38}

³⁶ A. U. Mac Rae, *Surface Sci.* **1**, 319 (1964).

³⁷ H. D. Hagstrum, *Phys. Rev.* **104**, 1516 (1956).

³⁸ H. D. Hagstrum, *J. Appl. Phys.* **32**, 1015 (1961).

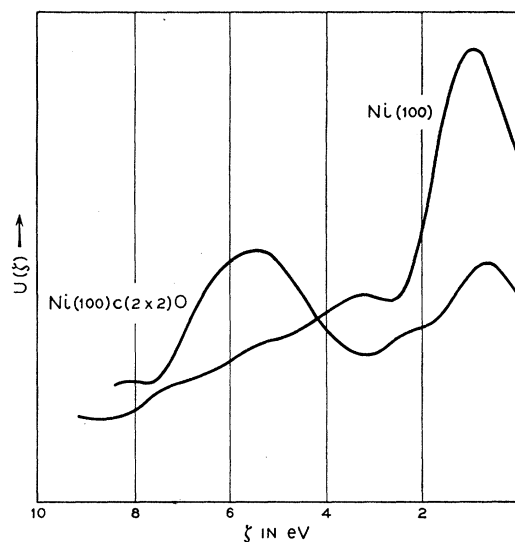


FIG. 20. Unfold functions $U(\zeta)$ derived from the $X_0(E)$ functions of Fig. 19.

XI. CHARACTERISTICS OF ION-NEUTRALIZATION SPECTROSCOPY AND COMPARISON WITH OTHER SPECTROSCOPES

Ion-neutralization spectroscopy is a procedure for deriving a function $U(\zeta)$ from experimentally determined energy distributions $X_K(E)$ of the ion-neutralization process. In this section we summarize the characteristics of INS and compare it, where appropriate, with other spectroscopies of the solid state, namely, the soft-x-ray spectroscopy (SXS) and the photoelectron spectroscopy (PES).

(1) *Density of initial states.* Although there are strong and characteristic transition probability factors, we have seen that when the crystal surface is atomically clean the bulk density of initial states plays a large role in determining the structure of the $U(\zeta)$ function. d -band electrons are clearly visible in the $U(\zeta)$ for copper and nickel, Fig. 14, but their intensity is reduced relative to the s - p band. Similarly, the degenerate p band of diamond-type semiconductors as will be reported elsewhere, can be seen. Thus INS, like SXS and PES, provides information about bulk density of states. The transition-rate factors [items (3) and (4) below] show interesting differences, however.

Also of interest is the question as to whether INS will detect many-body resonances as have been discussed by Spicer and collaborators^{39,40} and by Hopfield.⁴¹ As will be discussed in more detail elsewhere, no resonance below the d band was found in Ni although

³⁹ C. N. Berglund, in *Optical Properties and Electronic Structure of Metals and Alloys, Proceedings of the International Colloquium, Paris, 1965* (North-Holland Publishing Company, Amsterdam, 1966), p. 285.

⁴⁰ W. E. Spicer, in Ref. 39, p. 296.

⁴¹ J. J. Hopfield, *Phys. Rev.* **139**, A419 (1965).

there is some evidence of low-lying peaks in Cu which differ in position with crystal face. It is not inconceivable that transition-probability characteristics of INS will preclude the observation of resonances which are detectable photoelectrically. Mott⁴² has suggested that the positive charge of the incoming ion will repel the d -band hole on a Ni atom whose presence is required to produce the resonance observed by PES. Spicer⁴³ has suggested that a charged atom will draw its wave functions closer to itself and thus possibly not be detectable at the ion position. We cannot attribute the failure to observe the low-lying resonance in Ni to the inability of INS to see a peak which is deep in the band in view of the results for the surface crystal discussed in Sec. X.

It was pointed out in Sec. VIII that the ion-neutralization process favors the involvement of band electrons moving in the crystallographic direction normal to the sample face at which ion neutralization takes place. Thus INS tends to give one information on the bulk density of states of \mathbf{k} vector normal to the surface of the sample used. This is an interesting result in view of the known fact that the density of states normal to the surface does not enter into the tunneling rate through a thin barrier. The semiconductor presents an interesting special case in that filled surface states in the forbidden gap or states restricted to the surface by band bending should be detectable by INS. Semiconductors studied to date have had p -type surfaces where *bona fide* surface states lie above the Fermi level and are unfilled. Study of a semiconductor surface which has filled surface states of density approximating one per atom is of great interest. Since it appears that both electrons in the ion-neutralization process originate at the surface, band bending would have to be extremely severe before its effect could be detected by INS.

(2) *Density of final states.* There is no evidence that the use of INS to date has revealed any features attributable to the density of final states. This is inextricably tied up with the escape probability as the other principal dependence on final-state energy. SXS used in absorption gives direct data on final-state densities. PES also gives results interpretable as variations in the density of final states.⁴⁴ The rationale behind the extraction of information concerning final-state density from INS is the same as that for PES. In PES a large number of photon energies may be used. In INS only 2 or 3 equivalent input energies may be used for different noble-gas ions.

(3) *Transition probability factors for the clean surface.* The principal factors here are a tunneling factor decreasing with increasing depth in the band (ζ) and a symmetry factor decreasing as the character proceeds from s to p to d , etc. Results appear to be consistent

with approximately equal factors applied to both "down" and "up" electrons or with $U(\zeta)$ being a mean between somewhat divergent $U_1(\zeta)$ and $U_2(\zeta)$ functions for the two participating electrons. Also, no effects have as yet been observed which are attributable to final-state interactions of the ion-neutralization process.

Transition-probability factors can be affected by the presence of excited states (most likely broadened by interaction with the solid) in the atomic well lying opposite filled levels in the solid. The anomalies observed for Ne, which has the lowest lying excited levels, imply that the ionization limit of all the noble-gas atoms are most likely accounted for by these states. Electrons tunneling into excited states greatly enhance the transition probability for the range of ζ over which this is possible. This restricts the use of INS to solid surfaces for which φ is large enough to put the Fermi level below the lowest lying excited atomic level of the neutralized atom at the ion-solid separation at which neutralization occurs.

Except for the case of increased probability of transition for electrons moving normal to the surface, little in the way of momentum conservation is expected in INS. This results from the fact that the atomic ground state can absorb large amounts of momentum. In this regard INS might well differ considerably from SXS and PES although in the latter case momentum non-conservation appears also to play an important role.⁴⁵

(4) *Additional transition probability factor for the surface containing foreign atoms.* Foreign atoms incorporated in a reconstructed, crystallographically ordered surface monolayer or in an amorphous layer can alter the dependence of transition probability on band energy. From this it appears possible to delineate the energy profile of this property of the surface crystal. This fact puts a stringent requirement on surface cleanness of the sample if bulk properties are to be studied, but offers the further possibility of electronic spectroscopy of the surface which is unavailable to SXS or PES. Thus INS offers the attractive possibility of studying the electronic band structure as defined in this paper of extremely thin layers of one material upon another and of the nature of the band-structure transition from one solid to another. In the present apparatus growth of one solid upon another, whether epitaxial or amorphous, could simultaneously be followed by INS and LEED over the range from a fraction of a monolayer to films of any desired thickness.

(5) *Effect of different ions.* In PES photon energy may be changed essentially continuously. The equivalent photon energy in the ion-neutralization process is the energy $E_i' - \varphi$ which may thus be varied only by changing ions. In principle it would be possible to use many different ions, but because of the possibility of adsorption of the parent gas on the target surface we have limited ourselves to the noble gases and hence to only a few equivalent photon energies. This is possibly a

⁴² N. F. Mott, *Advan. Phys.* **13**, 325 (1965); in Ref. 39, p. 314; and private communication.

⁴³ W. E. Spicer (private communication).

⁴⁴ N. B. Kindig and W. E. Spicer, *Phys. Rev.* **138**, A561 (1965).

⁴⁵ W. E. Spicer, *Phys. Rev. Letters* **11**, 243 (1963).

disadvantage of INS. He^+ provides the largest equivalent photon energy, giving $E_i' - \varphi \sim 22.5 - 4.5 \sim 18$ eV for a solid having a 4.5-eV work function. This is large compared to the photon energies which have been used to date in PES when ultrahigh vacuum is desired. Of course if one dispenses with windows and can tolerate "monochromator vacuum," PES can be carried to much higher photon energies.

(6) *Effect of different crystal faces.* For atomically clean surfaces there is little *a priori* reason to expect different transition-probability factors for different crystallographic faces. Work to date bears this out. However, the effect of greater transition probability for band electrons moving normal to the surface will produce differences, as has been pointed out in Sec. VIII. [Item (1) above.] Such effects have been seen in the results for both metals and semiconductors.

For surfaces containing foreign atoms, different crystal faces could form different two-dimensional structures involving the same foreign atom. These surface crystals would in general have differing band-pass characteristics which can be studied by INS.

(7) *Energy broadening and its removal.* The ion-neutralization process has a considerable amount of energy broadening attributable to several causes. The extrapolation used to reduce the broadening works well except at the high-energy end of the $X_K(E)$ distribution. Here it is tied in with the problem of locating the Fermi level. Energy-broadening effects are serious in SXS, especially for solids of the heavier atoms where the situation is much more difficult than for INS. Final-state energy broadening becomes a nuisance in PES at higher photon energies, at least for cesiated surfaces. Final-state broadening exists in INS as in SXS and PES, but its magnitude has not been evaluated as yet.

(8) *Fermi-level location.* The Fermi level cannot be located directly and straightforwardly in INS by virtue of the energy broadening inherent in the process.

It is an absolute essential to start the $F(\xi)$ function properly, however, if it is to unfold. This is really a blessing in disguise because the necessity to make the starting portion of $F(\xi)$ consistent with the rest of the function does, in fact, help to locate the Fermi level. Location of the Fermi level is not particularly easy in SXS, especially for heavier materials. In PES the Fermi level can be located quite accurately.

(9) *Effect of escape probability.* The procedures of INS provide a way to determine a three-parameter escape probability. The large effective photon energy of

the process for He^+ ions means that one can investigate a band structure to a point 10 eV below the Fermi level and still remain almost 4 eV away from the vacuum level. This is a distinct advantage of INS over PES when LiF windows are used. Then important portions of the data lie immediately above the vacuum level where the $P(E)$ function varies rapidly. SXS has no equivalent problem.

(10) *Effect of inelastic scattering.* Although present, inelastic scattering appears to be small in INS by virtue of electron excitation near the surface. This is a definite advantage since it reduces final-state lifetime broadening and avoids a pile-up of slower electrons which tends to obscure structure deeper in the band. Inelastic scattering is appreciably less in INS than in PES used with cesiated surfaces.

(11) *Effect of unfolding.* In principle the necessity to unfold in INS must be listed as a disadvantage. Unfolding raises the basic questions of the difference in transition-probability factors for the "up" and "down" electrons concerning which we have only indirect evidence. Unfolding requires precise and relatively smooth data and thus decreases energy resolving power somewhat.

(12) *Resolving power.* At the moment it appears that we cannot expect a better resolving power for INS than a few tenths of an eV. Thus the value of INS might well lie in delineation of the coarser features of band state densities. Comparison with SXS would indicate SXS superior for the elements lighter than calcium, INS for the heavier elements. PES has a resolving power superior to INS except when electron-scattering effects are important.

ACKNOWLEDGMENTS

The author has profited greatly from conversations with a number of his colleagues, in particular, C. Herring, E. O. Kane, C. Semmelman, L. R. Walker, and M. C. Gray, to all of whom he expresses his thanks. The experimental data used here were obtained in collaboration with G. E. Becker, D. D. Pretzer, and Y. Takeishi, as indicated in Sec. I. Several persons have helped in writing the programs used in processing the digital data. In particular, thanks are due Miss Irene Bogdanski and Miss Rosemary Cox. Others whose help or guidance is appreciated have been mentioned in the body of the text. The author is also grateful for critical comments on the manuscript from E. G. McRae, G. E. Becker, and W. E. Spicer.